Materials Sciences Corporation

ENERGY DISSIPATION CHARACTERIZATION AND DESIGN METHODOLOGY FOR COMPOSITE MATERIALS

Technical Final Report

MSC TFR 3610/AA20

November, 1996

Contract No. N00019-96-C-2028

Contract Dollar Value: $69,892

Competitively Awarded

DISTRIBUTION STATEMENT A: Approved for Public Release
Distribution is Unlimited

SPONSOR: Mr. William McGannon
Naval Air Systems Command
AIR 4.3.4/WM
Arlington, VA 22243-5120

Suite 250, 500 Office Center Drive
Fort Washington, PA 19034
Tel: 215-542-8400 Fax: 215-542-8401

REPORT DOCUMENTATION PAGE	*Form Approved OMB No. 0704-0188*

1. AGENCY USE ONLY (*Leave blank*)	2. REPORT DATE	3. REPORT TYPE AND DATES COVERED
	November 1996	Final Report - 5/96 - 11/96

4. TITLE AND SUBTITLE

Energy Dissipation Characterization and Design Methodology for Composite Materials

5. FUNDING NUMBERS

N00019-96-C-2028

6. AUTHORS(S)

Sailendra N. Chatterjee and Chian-Fong Yen

7. PERFORMING ORGANIZATION NAME(S) AND ADDRESS(ES)

Materials Sciences Corporation
500 Office Center Drive, Suite 250
Fort Washington, PA 19034

8. PERFORMING ORGANIZATION REPORT NUMBER

MSC TFR 3663/AA20

9. SPONSORING/MONITORING AGENCY NAME(S) AND ADDRESS(ES)

Mr. William McGannon
Naval Air Systems Command
AIR 4.3.4/WM
Arlington, VA 22243-5120

10. SPONSORING/MONITORING AGENCY REPORT NUMBER

11. SUPPLEMENTARY NOTES

12a. DISTRIBUTION/AVAILABILITY STATEMENT

Distribution Statement A; Approved for Public Release. Distribution is unlimited

12B. DISTRIBUTION CODE

13. ABSTRACT (*Maximum 200 words*)

Various damages, which develop in structural composites, cause a softening behavior which can cause significant load redistribution in non-critical as well as critical areas of various structural elements. The strain energy dissipation (SED) concept provides a set of consistent nonlinear constitutive relations for stress analyses and the in-plane loader (IPL) provides a way for material characterization. Damage surfaces for moderate values of dissipated energy densities (DED) were estimated to match the response of conventional $(\pm\theta)_{ns}$ coupon tests, which are influenced by matrix mode damages. Softening behaviors for high values of DED which can result from fiber breakage/pull out were estimated using engineering judgement. Nonlinear finite element analyses were performed for two classes of structural elements; namely, (i) a $(\pm\theta)_{ns}$ cylindrical pressure vessel, where the nonlinearities in load-deformation responses are noticeable before fiber failure, and (ii) open hole tension of two quasi-isotropic layups, where local failure and softening in the fiber direction become critical to cause catastrophic failure. The results show the usefulness of the approach for design purposes and for explaining the complex problem of the so called "hole size" effect. Extension of the SED concept to the 3-D problem is suggested and a new approach to the problem of certification is discussed. Usefulness of the data generated by the IPL could not be assessed since they were not available for use. However, it appears that such data would be useful if they can provide full information up to high DED levels required for complete softening due to fiber breakage and pull out. Additional studies are suggested for the following phases for utilizing the full potential of the approach. Use of the test devices (IPL) and/or other tests by other testing organizations are also recommended to determine their acceptability and versatility.

14. SUBJECT TERMS	15. NUMBER OF PAGES
Strain Energy Dissipation, Dissipated Energy Density, Stiffness Loss, Softening Behavior, Nonlinear Response, Multiaxial Stress States, Certification, Design	73
	16. PRICE CODE

17. SECURITY CLASSIFICATION OF REPORT	18. SECURITY CLASSIFICATION OF THIS PAGE	19. SECURITY CLASSIFICATION OF ABSTRACT	20. LIMITATION OF ABSTRACT
UNCLASSIFIED		UNCLASSIFIED	

NSN 7540-01-280-5500

Standard From 298 (rev. 2-89)
Prescribed by ANSI Std. Z39-18
298-102

PREFACE

This work was performed by Materials Sciences Corporation (MSC) under SBIR Phase I, Contract No. N00019-96-C-2028, from Naval Air Systems Command. Dr. Sailendra N. Chatterjee was the principal investigator at MSC. Dr. Chian-Fong Yen also contributed to the work reported herein. Mr. Marc Portanova (Code 4.3.4.3) of NAWC AD, Pax River, MD, and Mr. William McGannon (AIR 4.3.4/WM) of NASC, Arlington, VA, were the technical points of contact.

TABLE OF CONTENTS

INTRODUCTION

Current methodologies for design of composite structures employ stress analyses with appropriate factors of safety for different kinds of failures (fiber or matrix dominated). A series of material characterization tests is needed to determine various strength characteristics and elastic properties of candidate unidirectional and/or laminated composites. In addition, knock-down factors are often used to account for stress concentrations near holes, notches or cut-outs, and again tests are needed to determine these factors. As a result, the whole process of structural design and material/laminate selection is time consuming and expensive. In addition, since such designs are based on elastic analyses without due consideration of nonlinear material response due to damage growth and the resulting load redistribution (especially near points of stress concentration), the process often yields overly conservative designs. With the increase in the efficiency of finite element methods applied to inelastic stress analyses of composite structures, there remain two main stumbling blocks for obtaining cost effective, but optimized design of composite structures; namely (i) quick and inexpensive material/laminate property characterization well in the nonlinear region, and (ii) suitable constitutive laws to model such nonlinear material responses.

The strain energy dissipation (SED) concept proposed by researchers at the Naval Research Laboratory (NRL) [1-4] provides a basis for quick characterization of candidate material systems under multiaxial in-plane loads. In this approach, strain energy dissipation in notched laminate specimens subjected to in-plane loads are evaluated experimentally for fifteen chosen loading paths. Computational procedures are suggested for determination of the dissipated energy density function [2] and laminate constitutive relations [4]. Finite element analysis is needed for performing these procedures. The work reported to date employs elastic stress analyses. It is suggested that such analyses may be adequate unless one ventures deeply into the nonlinear regime. Nonlinear stress analyses and a number of iterations will be needed in such regimes. A different loading system (as opposed to the in-plane loader IPL) and associated data analysis procedures are currently under development for complete three-dimensional characterization. It may be noted that test data generated on $(\pm\theta)_{ns}$ specimens (with various values of θ) loaded by the IPL have been used by NRL researchers to obtain a constitutive law for a ply (in-situ). Although several inter-

nal state variables (or damage parameters) may be needed to completely model the material response in the nonlinear range, a single one (the value of the dissipated energy density) has been found to yield a good representation of $(\pm\theta)_{ns}$ laminate response under various multiaxial loading paths.

Experimental observations on composite laminates indicate various forms of damage in brittle matrix composites; namely, (i) ply cracks parallel to fibers, extending through the thickness of a ply and constrained by the fibers in neighboring laminae, (ii) delaminations between plies of different orientations (originating from ply cracks or from free edges), (iii) matrix cracks parallel to fibers, (iv) fiber breaks, (v) fiber/matrix debonds, and (vi) fiber microbuckling or kinking under compression, etc. Some of these damage modes are illustrated in Figures 1-4. In many cases, effects of these damages are obvious in the highly nonlinear load deformation or stress-strain responses (see, for example, Figure 5 [5]). Various studies are reported in literature, which have attempted to obtain "in-situ" ply constitutive laws with appropriately chosen internal state variables (damage parameters, such as ply and matrix crack densities or spacings [6-10], delamination and debond densities [9], local fiber rotations due to kinking [11], etc.). Various material parameters, such as critical energy release rates for ply and matrix cracking as well as delamination growth are needed for such models. Some of these parameters are difficult to obtain directly from tests and are often calculated to fit specimen responses dominated by a particular form of damage.

Composite design engineers are aware that some types of laminate characterization specimens do show considerable damage growth and highly nonlinear responses under certain loading conditions. A $(\pm45)_{ns}$ tension coupon used for characterizing the nonlinear shear response of the unidirectional material is an example (see Figure 5). On the other hand, tension or compression response of high modulus unidirectional or crossply coupons loaded in fiber dominated directions may not show any appreciable nonlinear response. Composite laminates used in aircraft structures are often fiber dominated, and for this reason aircraft engineers commonly use elastic theory for design purposes with due consideration to the nonlinear unidirectional response under shear and transverse tension. It may be noted that damages do occur in laminates under tension and/or compression loading in the fiber dominated directions, but they are masked by the high modulus fibers even up to the point of initial fiber failures, which quickly become catastrophic in coupon specimens.

These damages cause some load redistribution but play a minor role on failure. Near points of stress concentrations, such as holes, notches, or cut-outs, a significant amount of load redistribution is expected before failure. Therefore, an inelastic stress analysis that uses nonlinear ply constitutive laws would yield a more realistic representation of local load redistributions between the plies and from damaged areas to neighboring undamaged regions. Use of such analyses has so far been limited to research studies. Therefore, it appears worthwhile to investigate nonlinear ply or laminate constitutive laws based on the SED concept and the use of such laws and nonlinear analysis for design and certification of aircraft structures.

The work plan for the proposed Phase I effort was to use the material data base and the analytical tools developed at NRL for performing analog experiments on some currently used simple material characterization specimens (such as $(\pm 45)_{ns}$ tension coupon) as well as other structural elements where material nonlinearity may play an important role. Comparison of the results of such nonlinear and linear analyses as well as test data would then be made to examine the accuracy and benefits of the nonlinear material property characterization using the IPL, combined with the SED concept. Finally, possible approaches would be suggested for modification and use of the concept for design and certification.

Discussions with NRL researchers indicated that the data for strain energy dissipation for characterizing the nonlinear material responses are not available for use. Also, there does not exist an available subroutine for computation of strain level dependent nonlinear properties which can be used with standard finite element codes. NRL plans to make their simulation capability available to users on the Worldwide Web sometime in the future. For these reasons, the plan of work for the Phase I effort was modified as described below. Parameters describing the strain energy dissipation (SED) contours were estimated from nonlinear stress-strain responses of $(\pm\theta)_{ns}$ tension and compression tests reported in literature. In addition, an in-house finite element code was modified to perform nonlinear stress analyses.

PHASE I TASKS AND OBJECTIVES

The main objective of the effort was to evaluate the usefulness of material characterization in terms of dissipated strain energy density under in-plane loading and analyze the benefits of the approach for design and certification. The following tasks were performed to meet specific objectives.

Task 1. Review and Implementation of the SED Concept - This task was designed to review the principles and assumptions used in the approach and to develop a subroutine for obtaining the nonlinear constitutive law which can be used with a finite element code for stress analysis.

Task 2. Estimate SED Surfaces - The objective was to estimate the strain energy dissipation surfaces in the three dimensional strain space via correlation of simulation results with test data from $(\pm\theta)_{ns}$ carbon/epoxy tension and compression coupon responses.

Task 3. Analog Experiments for Structural Elements - These experiments were designed to study the effects of material nonlinearity on stress, strain, damage states, and load redistribution. Also, failure was to be characterized.

Task 4. Examine Advantages of the Approach - Based on the results of Task 3, examine the usefulness of nonlinear material characterization and stress analyses for design purposes and suggest any modification and improvements.

Task 5. Design/Certification Procedures - Suggest alternatives for demonstration and validation to be performed in the following phases.

DESCRIPTION OF WORK

TASK 1. REVIEW AND IMPLEMENTATION OF THE SED CONCEPT

Task 1.1 Review

As discussed in the previous section, strain energy dissipation in composite laminates occurs due to the development of various types of damages. Several assumptions in the SED approach have been mentioned by NRL researchers [1]. Some of the important ones are described below.

1. The laminate can be regarded as a mechanically equivalent homogeneous anisotropic material or plate.
2. Displacement continuity is maintained between the layers.
3. Unloading to zero load yields zero strains, i.e., residual processing stresses are absent and the damages are in the form of microcracks or similar defects.
4. Explicit load history or time dependent effects are absent.
5. Dissipated energy (as a function of strains) is independent of the loading path.

Validity of the last assumption can be checked only by correlation of calculated strains and displacements with a series of carefully conducted tests.

The fourth assumption is valid for many brittle matrix composites. It may not be appropriate for composites with some thermoplastic matrices. The approach may be modified to address this issue by adding the effects of plastic and time dependent responses to those due to damages, but procedures for data analysis will become extremely complicated.

Assumptions 1-3, however, are very restrictive. For example, the most common forms of damage in laminated composites are ply cracks parallel to fibers, whose spacing gradually increases with applied loading. However, interply delaminations are often generated from such ply cracks. Similarly fiber/matrix debonds are also known to develop from matrix cracks or fiber breaks. Residual processing stresses at ply or fiber/matrix level can be quite high in some new composites being considered for various applications. As an ex-

ample, some test results for a carbon/epoxy (AS4/3502) laminate [12] are shown in Figures 6a and 6b. Figure 6b clearly shows the effect of residual processing stresses (tensile in the 90° layers), which causes a nonzero strain at zero value of average laminate stress. This material has a curing temperature higher than that of AS4/3501-6. Ply cracks are often found in common carbon/epoxy composites even in the unloaded state because of residual stresses. These issues can be addressed only if a procedure is developed for obtaining "in-situ" ply level constitutive law from the strain energy dissipations measured from laminate specimens. It is now well known that such a law can not be obtained from tests on unidirectional specimens. The task is a complicated one, since each lamina may have its own damage state which changes with load type and intensity. NRL researchers suggest that a ply-level "in-situ" constitutive law can be obtained from tests on angle ply laminates which also removes the restriction imposed by the first assumption. It is known, however, that the two ply thick inner layer and the outer plies in symmetric angle ply laminates usually develop ply cracks earlier than the other plies. It is not clear how the results are affected by such differences in energy levels for damage initiation in different layers. Further, assumption 3, which is essential for determining the in-situ ply constitutive law, is violated by the growth of delaminations due to interlaminar stresses. However, such growth usually occurs well in the nonlinear regime and may not be important in the initial stages. Although the NRL work indicates that more than one damage parameter (or a damage vector) can be considered as state variables, the present approach employs one such parameter. Obviously data analysis procedures will be quite complicated if multiple damage parameters are utilized and no assumption is made regarding the physical process of damage growth and the damage pattern.

One problem which is not addressed in the NRL reports is the definition of failure. In some laminates, the stress-strain responses are highly nonlinear and failure may possibly be defined by some arbitrarily imposed limit on strain energy dissipation. However, in many fiber dominated laminates, which are commonly used in aircraft components, failure often occurs due to fiber fracture after a limited amount of inelastic behavior.

There are some additional questions which must be answered with regard to some key assumptions in data reduction procedures and specimens used in the In-Plane Loader (IPL).

a. Use of linear laminate theory for data analysis from tests on notched specimens.
b. Effects of small sizes of specimens and zones of high strains and stresses.
c. Effects of temperature and moisture.

Qualitatively, it appears likely that the approach will be a useful tool for assessing the effects of growing damages and associated nonlinear response of the material with increasing load. However, before the approach is used quantitatively for the purpose of design, a number of analytical evaluations will be required. As a starting point, it will be worthwhile to compare the SED simulation results using data generated with the IPL and notched specimens with the responses of some simple laminate coupons and structural components. Such data have been reported in literature or are available in data bases generated under various DoD sponsored programs. Such comparisons will help resolve the issues related to questions a and b mentioned above. These comparisons were originally planned for this work, but could not be attempted, since SED contours in the NRL data base were not available. As regards to question c listed above, it appears that the strain energy dissipation contours in the (mechanical) strain space must be considered to depend on temperature and moisture. However, tests at various temperature and moisture environments and data reduction procedures with due consideration to hygrothermal stresses will be needed for this purpose.

Some of the issues discussed above will be addressed again in the sections which follow.

Task 1.2. Implementation

Constitutive laws for modeling microcracking in a continuum are discussed in [13]. Such models have been found to be very successful representing the behavior of brittle materials and make use of a phenomenological approach and the internal variables ω^{α}, which are the damage variables (such as average crack densities). One can write the formulation given in reference 13 in the following form where $\underline{\sigma}$ and $\underline{\varepsilon}$ are vectors.

$\underline{\sigma} \cdot d\underline{\varepsilon} - \rho d\psi = d\phi \geq 0$; Clausius-Duhem inequality (see Figure 7)

ρ = mass density

$\underline{\sigma} = \underline{\sigma}\,[\underline{\varepsilon}, \omega^{\alpha}; \alpha = 1, 2, \ldots k]$

k = total number of damage variables

ψ = Helmholtz free energy

$= \psi\,[\underline{\varepsilon}, \omega^{\alpha}]$ (1)

$$\sigma_i = \rho \frac{\partial \psi}{\partial \varepsilon_i}$$

$\phi = \phi\,(\underline{\varepsilon}, \omega^{\alpha})$, the dissipated energy density

$$d\phi = \sum_{\alpha=1}^{k} R^{\alpha} d\omega^{\alpha} \geq 0$$

R^{α} = conjugate thermodynamic force, an energy release rate for the damage variable $\omega^{\alpha} = R^{\alpha}\,(\underline{\varepsilon}, \omega^{\alpha})$

$$= -\rho \frac{\partial \psi}{\partial \omega^{\alpha}} = \frac{\partial \phi}{\partial \omega^{\alpha}}$$

In the SED formulation employed in [1-4], there is one damage variable (k = 1) which is the dissipated energy density ϕ ($=\omega^1$) and for this case one may choose the following form for the Helmholtz free energy

$$\rho\psi = \frac{1}{2} C_{ij} \varepsilon_i \varepsilon_j - \int_{o}^{\phi_c} R(\varepsilon_i, \phi) d\phi \qquad (2)$$

where ϕ_c is the current value of ϕ and C_{ij} are the elastic stiffnesses. It follows from the expression for $R^1 = R$ in last of (1) that for damage growth to occur

$$R(\varepsilon_i, \phi) = 1 \qquad 3)$$

and when $R\,(\varepsilon_i, \phi) < 1$, no damage growth would occur. In [1-4], it is also assumed that the dissipated energy is a function of the strain variables (independent of the loading path) and complete unloading will occur in a straight line from the current strain state to the origin. Accordingly, R may be chosen as

$$R(\varepsilon_i, \phi) = |\varepsilon|^2 / r^2(\phi, \beta_\gamma) \qquad (4a)$$

where for the problem of plane stress,

$$|\varepsilon|^2 = \left(\varepsilon_1^2 + \varepsilon_2^2 + \varepsilon_3^2\right) \tag{4b}$$

and r is magnitude of radius vector to the point on the damage surface in the strain space defined by the value of ϕ and two surface coordinates β_γ (γ = 1,2). The subscript 1 refers to the fiber direction, 2 to the transverse direction, and 3 to in-plane shear.

$$\beta_\gamma = \varepsilon_\gamma / |\varepsilon| \quad ; \quad \gamma = 1,2 \tag{4c}$$

In [1-4], the damage surfaces are obtained numerically from analysis of data from notched $(\pm\theta)_{ns}$ specimens for various values of θ and different loading paths using a curve fitting procedure. Since the data were not available for use, a simple approach was used in this study to define the damage surfaces in terms of a limited number of parameters which were chosen to match the average stress-strain response of $(\pm\theta)_{ns}$ tension and compression coupons reported in literature. As will be discussed later, some assumptions were also made to simulate the softening behavior in the axial direction caused by progressive fiber breaks, which may be expected under strain controlled conditions [14]. To define the damage surfaces in terms of a limited number of parameters, one may define

$$\frac{1}{r^2(\phi,\beta_1,\beta_2)} = \frac{1}{2} f(\phi,\beta_1,\beta_2) \tag{5}$$

and

$$f = \left[a_{11}\beta_1^2 + b_1\beta_1^2 \operatorname{sgn}\beta_1 + a_{22}\beta_2^2 + b_2\beta_2^2 \operatorname{sgn}\beta_2 + a_{33}\beta_3^2 + 2a_{12}\beta_1\beta_2\right] \tag{6}$$

where

$$\beta_3^2 = 1 - \beta_1^2 - \beta_2^2 \tag{7}$$

a_{ij} and b_i are functions of ϕ and the function sgn denotes the sign of the argument. Since for damage growth R (ε_i,ϕ) = 1, equation (4a) yields

$$\frac{1}{2}\left[\varepsilon_1^2\left(a_{11}(\phi) + b_1(\phi)\operatorname{sgn}\varepsilon_1\right) + \varepsilon_2^2\left(a_{22}(\phi) + b_2(\phi)\operatorname{sgn}\varepsilon_2\right) + \varepsilon_3^2 a_{33}(\phi) + 2a_{12}(\phi)\varepsilon_1\varepsilon_2\right] = 1 \tag{8}$$

Equation (8) is similar to the Tsai-Wu type polynomial failure criterion, but it is in terms of strains and the coefficients a_{ij}, b_i are functions of ϕ. The linear terms used in Tsai-Wu type criterion are not used here since they give a strong coupling between shear stress σ_3 and the extensional strains ε_1 and ε_2 in the resulting stress-strain relation discussed later. More

complicated forms may be chosen if desired, but the representation (5,6) is quite adequate to fit available test data and for the analog experiments described later. It may be noted that $a_{33}(\phi)$ can be obtained if the nonlinear shear stress-strain response is known and ϕ can be calculated for various values of shear strain ε_3. Similarly, if unidirectional strain-stress responses in fiber (1) and transverse (2) directions are known (for example, σ_1 is known for various ε_1, when $\varepsilon_2 = 0$), then $a_{11}(\phi)$, $b_1(\phi)$ and $a_{22}(\phi)$, $b_2(\phi)$ can be evaluated as functions of ϕ. Such an approach was adopted for obtaining initial estimates of these coefficients for AS-3501, which were later adjusted to fit available test data.

Substitution of (4a), (5) and (6) in (2) yields

$$\rho\psi = \frac{1}{2}C_{ij}\varepsilon_i\varepsilon_j - \frac{|\varepsilon|^2}{2}F(\phi,\beta_1,\beta_2) \tag{9}$$

where

$$F = \left[\beta_1^2\left(A_{11}(\phi) + B_1(\phi)\operatorname{sgn}\beta_1\right) + \beta_2^2\left(A_{22}(\phi) + B_2(\phi)\operatorname{sgn}\beta_2\right) + \beta_3^2 A_{33}(\phi) + 2\beta_1\beta_2 A_{12}(\phi)\right] \tag{10}$$

$$A_{ij}(\phi) = \int_0^\phi a_{ij}(\phi)d\phi \tag{11}$$

$$B_i(\phi) = \int_o^\phi b_i(\phi)d\phi \tag{12}$$

Using the expression in (1) for evaluation of σ_i as a derivative of $\rho\psi$, one obtains

$$\sigma_i = C_{ij}\varepsilon_j - \varepsilon_i F - |\varepsilon|\left(\delta_{i\gamma} - \varepsilon_i\varepsilon_\gamma / |\varepsilon|^2\right)\frac{1}{2}\frac{\partial F}{\partial\beta_\gamma} \quad ,i = 1,2,3 \tag{13}$$

where the repeated index γ implies summation over $\gamma = 1$ and 2 and

$$\frac{1}{2}\frac{\partial F}{\partial\beta_1} = \left(A_{11} + B_1\operatorname{sgn}\beta_1 - A_{33}\right)\beta_1 + A_{12}\beta_2 \tag{14}$$

$$\frac{1}{2}\frac{\partial F}{\partial\beta_2} = A_{12}\beta_1 + \left(A_{22} + B_2\operatorname{sgn}\beta_2 - A_{33}\right)\beta_2 \tag{15}$$

where A_{ij}, B_i are functions of ϕ. The kronecker δ in (13) is

$$\begin{aligned}\delta_{i\gamma} &= 1 \qquad i = \gamma \\ &= 0 \qquad i \neq \gamma\end{aligned} \tag{16}$$

The constitutive relations described above and the iterative procedures required for evaluation of current value of dissipated energy (using the condition $f = 2/|\varepsilon|^2$) were incorporated in a subroutine, which is used with a finite element code [15].

For a clearer explanation of the parameters, one may consider the stresses for the following loading paths. The constitutive relation yields the following results for the chosen paths.

A. $|\varepsilon_1|$ increasing, $\varepsilon_2 = \varepsilon_3 = 0$

$$\sigma_1 = (C_{11} - A_{11}(\phi) \mp B_1(\phi))\, \varepsilon_1 \qquad (17)$$
$$\sigma_2 = (C_{12} - A_{12}(\phi))\, \varepsilon_1$$
$$\sigma_3 = 0$$

Negative sign in first of (17) applies for positive ε_1 and positive sign is for negative ε_1. Thus $(A_{11} \pm B_1)$ denote the stiffness loss in direction 1 and A_{12} quantifies the reduction in the cross term. Similarly, the following results are self-explanatory.

B. $|\varepsilon_2|$ increasing, $\varepsilon_1 = \varepsilon_3 = 0$

$$\sigma_1 = (C_{12} - A_{12}(\phi))\, \varepsilon_2 \qquad (18)$$
$$\sigma_2 = (C_{22} - A_{22}(\phi) \mp B_2(\phi))\, \varepsilon_2$$
$$\sigma_3 = 0$$

C. $|\varepsilon_3|$ increasing, $\varepsilon_1 = \varepsilon_2 = 0$

$$\sigma_1 = \sigma_2 = 0 \qquad (19)$$
$$\sigma_3 = (C_{33} - A_{33}(\phi))\, \varepsilon_3$$

Thus, A_{ij} and B_i define appropriate stiffness losses and a_{ij}, b_i are their derivatives with respect to ϕ. a_{ij}, b_i are needed for evaluation of ϕ for any loading path.

It is obvious that complete stiffness loss (describing full loss in load carrying capacity) will occur when the stiffness losses will equal the initial stiffnesses. Thus, for large values of ϕ, they should approach the corresponding initial elastic stiffnesses. Since the stiffnesses in directions other than the fiber direction (1) are much lower, the dissipated energy required for complete stiffness loss in those directions will be much lower than that for direction 1. Further, under transverse tension, stiffness loss is expected to occur at a much faster rate than that under transverse compression. This discussion should be useful in

understanding the reasons for the choices of the coefficients $a_{ij}(\phi)$ and $b_i(\phi)$ described in the next section.

TASK 2. ESTIMATE SED SURFACES

These estimates were made for a carbon epoxy composite (AS/3501) with elastic moduli and Poisson's ratio given in Table 1, which also gives the coefficients a_{ij} and b_i for various values of ϕ. As mentioned earlier, iterative procedures were used for determining the dissipated energy ϕ for increasing strains. Linear interpolation is employed in the code for determining the coefficients for intermediate values of ϕ and trapezoidal rule is used to integrate these values up to the current value of ϕ. The integrated values are listed in Table 3 along with their limits (the initial stiffnesses C_{ij}), which show that effective transverse and shear stiffnesses are reduced to zero much earlier than the axial stiffnesses. The coefficients a_{33}, a_{22} and b_2 were chosen so as to yield reasonable fit to average stress-strain response of $(\pm 45)_{ns}$, $(\pm 50)_s$ and $(\pm 30)_s$ tension coupons. Use was made of AS4/3501 $(\pm 45)_{ns}$ data in [5] and [16] and AS1/3501 $(\pm 50)_s$ and $(\pm 30)_s$ data given in [17]. It may be noted that $(\pm 45)_{ns}$ response is dominated by shear, whereas $(\pm 50)_s$ and $(\pm 30)_s$ results are affected by shear as well as transverse tension and compression, respectively. Nonlinear iterative analyses were performed on a single element model for performing the fits. Analysis of results with chosen properties (Table 1) are compared in Figures 8a, 8b, 9 and 10. The agreement is reasonable for low axial strain levels in $(\pm 45)_{ns}$ coupons (Figures 8a and 8b) and up to experimental failure strains for $(\pm 50)_s$ specimens (Figure 9). At high axial strain levels (above 2%) in $(\pm 45)_{ns}$ coupons, the values of assumed coefficients yield stresses which are lower than test data (Figure 9) for thicker specimens ($\geq$ 16 plies). Geometry changes (scissoring) may occur after gradual development delaminations, which may cause some stiffening in thick specimens. Thin specimens (8 plies) possibly fail quickly due to complete delamination before such stiffening can occur. Possibly for the same reason $(\pm 50)_s$ specimens fail early (Figure 10). On the other hand, measured $(\pm 30)_s$ response is above the analysis results for higher strain levels ($>$ 0.9%, Figure 10). Scissoring is possibly the reason for this difference.

Detailed response of $(\pm\theta)_{ns}$ compression coupons of AS/3501 material are not known to the authors. Responses of $(\pm 60)_{ns}$, $(\pm 30)_{ns}$ and $(\pm 20)_{ns}$ are compared with those reported in

[18] for AS/3502 in Figures 11 and 12. Axial failure stresses and strains for $(\pm 60)_{ns}$ are higher than the range plotted in Figure 11, but those for $(\pm 30)_{ns}$ and $(\pm 20)_{ns}$ (Figure 12) are lower than those computed. Existence of transverse tensile stresses and early development of delamination are possibly the reasons for these differences.

Maximum values of computed dissipated energy densities in each of the layers of the $(\pm\theta)_{ns}$ coupons discussed in this section are listed in Table 3, which are quite low indicating that, as expected, these specimens do not show any fiber damage.

The coefficients a_{12} are chosen so as to simulate the changes in transverse strain (Poisson strain) observed in crossply $(0/90)_{ns}$ laminates loaded in axial tension. As an illustration, the average axial stress and transverse strains are plotted against axial strain in Figures 13a and 13b, respectively. Figure 13b illustrates how the transverse strain shows a strong nonlinear behavior at high axial strain levels. Also shown in the figures are some test data [16]. The specimens used had a higher fiber volume fraction (and a higher modulus in the fiber direction) than the value assumed here and hence they show a stiffer response. Calculated average stresses show a peak value of about 133 ksi at a strain level of 1.5% and then the stress gradually decreases as the strain increases. Such load drops and gradual softening (as assumed in the model) can only be observed in very carefully conducted displacement controlled tests. It should be emphasized that the actual softening behavior is difficult to quantify directly. Attempts have been made for their indirect quantification through analyses and correlation of observed response of notched fiber dominated layups [14]. However, the analytical model used in [14] for that purpose is different from the one used here and, therefore, it is not possible to compare the softening pattern used in [14] with the one employed here. Figure 14 shows the axial stress in the 0° layer in a $(0/\pm 45/90)_{ns}$ laminate subjected to axial strain (average transverse stress = 0) up to a strain level of 6%. This gives an idea of the softening pattern employed in this study. The dissipated energy in the 0° layer at 6% axial strain level is 7128 lb/in^2 (the maximum value used in calculation is 7500 lb/in^2, see Table 1). Such high strain levels and energy loss are indicative of lots of progressive fiber breaks and fiber pull out before final separation. Obviously, it is possible to perform calculations with different assumed softening behavior in terms of the assumed coefficients for high values of ϕ (see Table 1) to match data from different tests and to model the behavior up to complete separation (reduction of axial stress to zero), but such an effort is beyond the scope of Phase I work.

The values of coefficients given in Table 1 were used in the next section to study some sample problems to examine the usefulness of the concept. For completeness, we report here that the peak values of average laminate stresses for axial straining (with zero transverse stress) for $(0/\pm45/90)_{ns}$ and $(0/\pm60)_{ns}$ laminates are 98 ksi and 96.8 ksi, respectively, which occur at a strain level of 1.5% (which is the same for a $(0/90)_{ns}$ layup).

Before concluding this section, we note that under compressive loading the axial stress in the 0° layers in a crossply ($(0/90)_{ns}$) or a quasi-isotropic ($(0/\pm45/90)_{ns}$ or $(0/\pm60)_{ns}$) laminate show a softening behavior similar to that under tension shown in Figure 14, but the stresses are slightly higher for the same strain level except in the initial linear range. The coefficients are chosen to yield such a behavior, since constrained in-situ compression response show a slower rate of stiffness degradation after the peak [11].

TASK 3. ANALOG EXPERIMENTS FOR STRUCTURAL ELEMENTS

To examine the usefulness of the concept, two types of analog experiments were conducted as described below.

1. Elements showing noticeable nonlinear response before failure - The $(\pm\theta)_{ns}$ coupons analyzed in the previous section fall in this category but they are not common structural elements. Most possibly the simplest structural element in this category is a cylindrical pressure vessel (with closed ends) of $(\pm\theta)_{ns}$ construction commonly manufactured using the filament winding technique. Therefore, this element was considered for analysis in this category.

2. Elements where the effects of nonlinearities are masked before peak loads are reached - $(0/90)_{ns}$, $(0/\pm45/90)_{ns}$ or $(0/\pm60)_{ns}$ tension (or compression) coupons considered in the previous section belong to this class and the results show that the peak stresses can be predicted using this approach. However, it is known that the use of the linear theory with a prescribed fiber strain limit (1.3%, for example) will also yield acceptable results in these cases. Possibly the most common element where such a linear theory will not be useful is a tension or compression coupon with a stress raiser, a notch, a hole, or a crack. In the composites industry, the load carrying capacity of such an element is often predicted using the Whitney-Nuismer criterion [19], which was motivated by what is known

as the hole-size effect. Parameters required in the model have to be determined by fitting test data to the model and hence the approach is semi-empirical. A review of various other criterion suggested for the problem can be found in [20]. Tension coupons with two hole sizes were analyzed in this study to examine the usefulness of the SED concept in this problem. Most possibly this is a very severe test for the concept.

Results for the two types of elements are discussed next.

Task 3.1 $(\pm\theta)_{ns}$ Cylindrical Pressure Vessel

In the cylindrical region of a closed end pressure vessel, the state of stress is known, i.e., the axial tensile stress σ_A is half of the hoop tension σ_H. It is a common design practice to optimize the fiber orientation θ using the concept of netting analysis, which assumes that at the point of failure the layers carry stresses σ_1 only in the fiber direction (load carrying capacities in shear and transverse tension are destroyed), which yields

$$\sigma_H = \sigma_1 \cos^2\theta$$
$$\sigma_A = \sigma_1 \sin^2\theta \qquad (20)$$

Since $\sigma_A = \sigma_H/2$, one obtains the optimum fiber angle

$$\tan\theta = \sqrt{2}$$
$$\theta = 54.7356^o \qquad (21)$$

For simplicity, a single element model was analyzed for various imposed σ_H and σ_A ($= \sigma_H/2$) till peak stresses were reached, which occurred at

$$\sigma_H = 162.63 \text{ ksi}$$
$$\sigma_A = 81.315 \text{ ksi} \qquad (22)$$

Beyond this level the stresses could not be increased because softening started in the fiber direction.

The stress in the fiber direction σ_1 and the dissipated energy density ϕ for various values of σ_H are plotted in Figure 15a. The stress σ_1 for high values of σ_H approaches the netting analysis solution. ϕ is found to increase rapidly for high values of σ_H reaching a value of 281 lb/in^2, which implies that damages so far possibly do not involve fiber breakage, but some softening in the axial directions. Values of hoop strain ε_H and axial strain ε_A are plotted against σ_H in Figure 15b. The results show noticeable nonlinear responses for high val-

ues of σ_H. Use of netting analysis yields a laminate stiffness matrix A, which is singular. Use of appropriate limits, however, yields

$$\varepsilon_H = \varepsilon_A = \varepsilon_1 = \varepsilon_2 = 3\sigma_H / 2E_1$$
$$\gamma_{AH} = \varepsilon_3 (= \gamma_{12}) = 0 \qquad (23)$$

as the result of netting analysis (also shown in Figure 15b). The result is different from the calculated values (from nonlinear analysis) of ε_A and ε_H, which are quite different from each other. It should be noted that the layer stresses and strains at peak loads are as given below.

σ_1 = 242 ksi	ε_1 = 1.48%	
σ_2 = 1.92 ksi	ε_2 = 1.32%	(24)
$\sigma_3 = \tau_{12}$ = ±0.68 ksi	$\varepsilon_3 = \gamma_{12}$ = ±0.46%	

It is clear that σ_2 and σ_3 are small, but the state of strain is quite different from equation (23). If there is no softening in the axial direction, then the state of strain predicted by netting analysis may be the asymptotic solution at higher load levels.

Task 3.2. Tension Coupons with Holes

Tension coupons 1.5" wide and 6" long were considered in this subtask. Circular holes of diameter 1/4" and 1/8" at the center of the coupon (center of the hole is the origin x = 0, y = 0) were considered. Tensile load was applied by prescribing equal and opposite longitudinal displacements (u_x) at the two ends. The other displacement component u_y was assumed to be zero at these ends simulating clamping effects. The laminates were assumed to have a thickness of 0.04". Only a quarter of the coupon was analyzed because of symmetry about the planes x=0 and y=0. Finite element meshes near the hole are illustrated in Figures 16 and 17, respectively. Elements close to the hole have the following dimensions in radial direction.

Row 1	.01"
Row 2	.02"
Row 3	.04"
Row 4	.045"

In the circumferential direction, they cover an angle of $\pi/32$ radians (16 elements in the quarter). Two quisotropic layups were analyzed, namely, $(0/\pm45/90)_s$ and $(0/\pm60)_s$. Loads were applied to a maximum value such that the dissipated energy density in a layer of the most critical element reached a value of 7500 lb/in^2 (the limit assumed in the properties as shown in Table 1). Load displacement plots and dissipated energy densities in each layer of some critical elements are shown in various figures described in Table 4. The critical elements are discussed next (see Figures 16, 17).

Elements	Row	Circumferential Position
1	1	Adjacent to plane x = 0
17	2	
33	3	
2	1	Next to element 1
18	2	Next to element 17
34	3	Next to element 33

As the load deflection plots (Figures 18, 23, 28 and 32) indicate, there are no appreciable nonlinearities even at the highest load level. However, the dissipated energy densities in various layers of the critical elements are of interest.

At maximum load for the $(0/\pm45/90)_s$ layup with 1/4" hole, the DED (Dissipated energy density) in the 0° layer in element 1 has a value of 7500 lb/in^2 as shown in Figure 19. In elements 17 and 33, the DED in 0° layers have not reached the maximum, but they are increasing at a fast rate. DED in the +45° and -45° layers of elements 1, 17 and 33 are also increasing rapidly (Figures 20, 21), whereas DED in the 90° layers have reached values of the order of 100 to 300 lb/in^2, indicating nearly complete loss in transverse stiffness. The situation is analogous to a plane of separation developing through elements 1, 17 and 33, which are closest to the plane x = 0. DED in the elements above this set, 2, 18 and 34, on the other hand, do not show any increase with load (near the maximum load level) indicating the effect of separation below. It appears, therefore, that a catastrophic failure is expected very close to the load level reached. For all practical purposes, this level may be considered as the failure load. For the case of 1/8" hole (Figures 23 -

27), the situation is similar except for the fact that the elements 2, 18 and 34 show highest values of DED in 0°, 45° and -45° layers and the values of DED in elements 1, 17, 33 have become fairly constant near the maximum load level. The strains ε_x in the most critical element for both hole diameters are of the order of 8%, which may be considered as separation.

For 1/4" as well as 1/8" hole in $(0/\pm 60)_s$ laminate, the DED in the 0° layer of element 1 (as in the case $(0/\pm 45/90)_s$ with 1/4" hole) has a value of 7500 lb/in^2 at maximum load and the 0° DED in element 17 is increasing rapidly. For +60 and -60 layers, the maximum values of DED are of the order of 500 to 600 lb/in^2 indicating some softening in these layers too. The DED in various layers of elements 2 and 18 do not show any increase with load near the maximum load level indicating the effect of separation in a plane passing through elements 1 and 17.

Maximum average stresses based on the gross cross-sectional area for the cases studied are given in Table 5. The results (normalized gross section stresses, σ_N/σ_o) are also plotted in Figure 36. σ_o, the unnotched strength, is taken as the peak stresses obtained from single element results reported in Task 2. Also shown in Figure 36 are the two bounds, one based on the assumptions of (i) no notch sensitivity (full ductility) and (ii) full notch sensitivity based on the stress concentration factor of 1/3. Usually test results for various hole sizes in such a figure are plotted after correcting the failure stress by the finite width correction factor based on elastic calculations. All results reported here are calculated, and no finite width correction factor is employed, because the material is not elastic. The results follow the trend of test data reported in literature. No systematic comparison with test results is reported here because of three reasons; namely, (i) the softening response in the fiber direction is assumed based on engineering judgement, (ii) detailed notched strength data for this system are not available, and (iii) test data are also strongly influenced by development of delaminations (and hence the lay-up sequence) and through the thickness effects are not addressed here. However, we note that 1.5" wide AS/3501 $(\pm 60/0)_s$ laminates with 1/4" holes tested at McDonnell Douglas yielded a mean gross section failure stress of 45.9 ksi with a standard deviation of 3.6 as compared to the calculated value of 49.3 ksi. Therefore, the properties used in this study are possibly not unrealistic.

TASK 4. ADVANTAGES OF THE APPROACH

The results for the filament wound pressure vessel problem (Task 3.1) indicates that the approach yields a good estimate of stiffness loss due to matrix mode damages (caused by transverse and shear strains) as compared to netting analysis. Calculated peak stress is close to that obtained using netting analysis. For its simplicity, the netting analysis will obviously be preferred for design purposes, but the peak value of fiber stress to be used for design is not necessarily the axial unidirectional strength (although it will be close to that value). However, if an estimate of strain and displacement fields is needed, the SED approach provides a much better estimate than that obtained from netting analysis.

The approach provides a consistent set of nonlinear constitutive laws for use in nonlinear finite element analyses. The second set of examples (Task 3.2) illustrates how the softening behavior in the axial direction influences the local field variables near a stress raiser and how separation caused by fiber breakage/pull out and similar damages can be simulated. Therefore, the approach provides a method to estimate various knock down factors employed for design. Obviously in the present form, the approach does not address the development of delaminations, which can play an important role on the failure near stress concentrations (especially for compression dominated loading where sublaminate buckling after development of delaminations can cause early failure), but it should be useful in reducing the number of tests required for assessing the influence of complicated phenomena such as the hole size effect. It is known that the damage zones near stress concentrations are often quite large in thin laminates mainly due to the development of delaminations. For moderately thick to thick laminates, effects of such damage zones are not that dominant. One of the main assumptions in the approach (in its present 2-D form) is that the laminate is not very thin and it contains dispersed layers arranged in a repeating pattern. Naturally it is not expected to simulate the three dimensional effects which are generated due to sharp gradients of in-plane stresses. It should be pointed out that the finite element code used in this study is three dimensional and makes use of brick type elements of thickness equal to the laminate thickness. Plane stress conditions were simulated by assuming that the through the thickness Poisson's ratios are zero. When these Poisson's ratios are not zero, high through the thickness stresses (extension or peel as well as two shear components) would be obtained in the critical elements. Effects of

these stresses and resulting damages can be assessed by extending the nonlinear constitutive law to the three dimensional problem. Determination of required material properties, however, will involve more complex procedures. Use of 3-D meshes and the increase in the number of degrees of freedom will increase the time and effort required for nonlinear finite element analysis by an order of magnitude or more. Usefulness and accuracy of the three dimensional formulation are yet to be explored.

It is clear from the results obtained that matrix mode damages which cause softening under the action of transverse strains and shear (although there is a coupling with axial strains too) cause dissipated energy densities which are low (maximum values are of the order of 200 lb/in^2). Material properties required in this range could be estimated from conventional test data (average stress vs. measured strain) from a limited number of $(\pm\theta)_{ns}$ tension and compression coupons of moderate sizes. These tests are easy to conduct and yield a reliable measure of the properties, since the states of strain and stress are uniform almost over the entire specimen. In this study the properties were estimated for a single material using nonlinear analyses and trial and error. An algorithm can be easily developed, if desired, to automate the process using the data for specimens with a finite number of values of θ to obtain the required damage surfaces. On the other hand, dissipated energy densities required to cause progressive fiber breaks and pull-outs are quite high (for this system it is of the order of 7500-10000 lb/in^2) and in this study, engineering judgement was used to estimate the required material properties for such high values of energy dissipation. It is obvious that no specimen with uniform strain/stress state can be designed to characterize this softening behavior, which can occur under highly constrained conditions. One possible approach for characterization of such softening is to make use of center notched fiber dominated layups such as $(0/90)_{ns}$, $(0/\pm45/90)_{ns}$, $(0/\pm60)_{ns}$ under tension and compression. These notches may be in the form of slits. It is known that a significant amount of nonlinearity is observed in the COD (crack opening/closing displacement) or NOD (notch opening/closing displacement) measured at the center of the notch. In contrast, there are no appreciable nonlinearities in the farfield load-displacement behavior. The process can again be automated, if desired. However, the nonlinearity is quite severe, since the release of high fiber direction stress is needed and, therefore, a complete nonlinear analysis would be required. For this reason, the procedure will not be very simple and

straightforward. It is not clear whether use of notched $(\pm\theta)_{ns}$ layups will yield the desired information.

It was not possible to examine the data generated at NRL from the notched $(\pm\theta)_{ns}$ specimens using the IPL and linear analyses. Results reported in [1-4] indicate that data are available up to dissipated energy densities of the order of 1000 lb/in^2 for AS4/3501-6 material. However, since the data are obtained from small size specimens with highly non-uniform strain/stress states, it would be difficult to convince the testing community of its acceptability unless it is shown that they can reproduce conventional test results from $(\pm\theta)_{ns}$ coupons. From data reported in [1-4], it is not clear whether the NRL database provides the information required for softening in the fiber direction. If it does, they will obviously be useful. However, the reliability of such data generated from linear analysis may again be questioned, unless their adequacies are demonstrated through additional tests and correlation studies.

Before concluding this section, we note that a major concern for the designers of composite structures is the effect of environment. Degradation of material properties (both stiffness and strength) under hot wet conditions is a major issue and often the designers attempt to address this issue relying on some critical tests under such conditions, such as open hole tension and/or compression. Determination of initial stiffnesses of the unidirectional material or the laminate at high temperature and moisture is always necessary (as in the case of room temperature), since these properties are essential for any analysis. The SED approach for nonlinear analyses can easily be extended to consider the environmental effects if the formulation is made in terms of mechanical strains (instead of total strains) and hygrothermal expansion properties are known. Effects of residual processing stresses are then easily considered. However, the damage surfaces must be treated as functions of temperature and moisture unless they are shown to be unaffected over the range of environment of interest. Available test data from $(\pm\theta)_{ns}$ coupons ($\pm$45 data are often used for characterization of shear properties) at elevated temperatures show significant differences from room temperature data in the linear as well as nonlinear ranges. Open hole tension test data at elevated temperatures also show some differences from such data at room temperature. Therefore, although the approach can be used to address the issue of changing environment, appropriate material characterizations under such environments will be needed.

TASK 5. CERTIFICATION ISSUES

There are various certification requirements, such as those required for material/laminate properties and part/subcomponent performances under quasi-static and repeated (fatigue) loadings under various environmental conditions. In addition, for composite aircraft, flight spectrum testing is often needed to address issues related to durability and fatigue.

As discussed earlier, tests for initial stiffnesses under various environmental conditions will always be required. Usefulness of the tests commonly performed for characterizing the strengths of the unidirectional material has been questioned by many. Obviously, transverse tensile strength determination is of little value. It is now recognized that for shear, nonlinear characterization is needed instead of the strength alone. Recent modifications to ASTM Standard D 3518 addresses this issue. Determination of high axial tensile or compressive strength from unidirectional specimens is a difficult problem and for this reason use of laminate tests (crossply, for example) has been suggested by many to determine the axial strengths in-situ. Therefore, addressing the certification issue in terms of laminate tests (some $(\pm\theta)_{ns}$, some fiber dominated) is worth considering. In the opinion of many experimentalists, "backing out" lamina strengths from laminate test results is unnecessary and fraught with uncertainties and there is no substitute for a good direct test [21]. However, if a series of laminate tests are proposed as a means of nonlinear material characterization under multi-axial loadings, then it may be possible to convince many that such an approach is worth pursuing. Therefore, the following approach may be suggested for certification tests.

1. Nonlinear material characterization for various environmental conditions - NRL specimens and IPL may be employed if these tests provide complete information including softening in the axial direction. Alternatively, conventional $(\pm\theta)_{ns}$ coupon tests and notched fiber dominated laminate tests can be used as suggested in the last section.

2. A limited number of open hole tension, compression and bolt bearing type tests under varying environments - Results from these tests must be correlated with analytical results using nonlinear properties obtained from test series 1.
3. A limited number of critical subelement/component testing for different environmental conditions which also must be correlated.
4. Additional tests to address the issue of fatigue.

It is not clear at this point how the fatigue issue can be addressed, i.e., either using the conventional approach or defining the damage surfaces as a function of loading cycles N and R ratio, i.e., r (ϕ, β_i, R, N). It is expected that substantial savings in time and expenses can be made if the present approach can be extended to the fatigue problem. However, the usefulness of the approach for fatigue is yet to be explored.

DISCUSSIONS

- Results of the Phase I study have shown that nonlinear constitutive laws defined in terms of a series of damage surfaces (for increasing dissipated energy densities) are useful and may be used to explain many complicated phenomena such as the hole size effect.
- Extending the approach to the three dimensional problem may be useful to address the effects of interlaminar damages (constrained delamination growth or separation) and may remove the restriction that displacement continuity between the layers has to be maintained.
- Such extension should be attempted in Phase II.
- Additional data correlation studies for open hole tension and compression, coupons with cracks and notches, as well as other critical elements, are needed using 2-D as well as 3-D formulations to demonstrate the full potential of the approach.
- Some suggestions have been made regarding certification tests. A full plan for a specific application should be developed in Phase II, and some representative certification authorities (DOD agencies, FAA and other) should be consulted for their opinion in this connection.
- It is recommended that the loading devices and test procedures be made available to one or more testing organizations so as to learn about their acceptability and ease of use. Generation of such material data by other users should also be attempted in Phase II.
- Attempts should be made to apply the approach to a few specific design and certification problems.
- No judgement could be made regarding the key assumption that the damage (DED) is independent of the path used to reach the current state of strain. Validity of this assumption can only be checked via carefully conducted tests using several alternative loading paths. It would be worthwhile to conduct such tests in Phase II.

REFERENCES

1. Mast, P.W., et al., "Experimental Determination of Dissipated Energy Density as a Measure of Strain-Induced Damages in Composites", NRL/FR/6383-92-9369.
2. Mast, P.W. et al., "Characterization of Strain-Induced Damage in Composites Based on the Dissipated Energy Density, Part I. Basic Scheme and Formulation", Theoretical and Applied Fracture Mechanics, Vol. 22, p. 71, 1995.
3. Mast, P.W., et al., "Characterization of Strain-Induced Damage in Composites Based on the Dissipated Energy Density, Part II. Composite Specimens and Naval Structures", Theoretical and Applied Fracture Mechanics, Vol. 22, p. 97, 1995.
4. Mast, P.W., et al., Characterization of Strain-Induced Damage in Composites Based on the Dissipated Energy Density, Part III. General Material Constitutive Relations", Theoretical and Applied Fracture Mechanics, Vol. 22, p. 115, 1995.
5. Kellas, S., Morton, J., and Jackson, K.E., "Damage and Failure Mechanisms in Scaled Angle-Ply Laminates", ASTM STP 1156, p. 257, ASTM, Philadelphia, 1993.
6. Chatterjee, S.N., Wung, E.C.J., and Yen, C.F., "Modeling Ply Crack Growth in Laminates Under Combined Stress-States", ASTM STP 1156, pp. 195-217, 1993.
7. Hashin, Z., "Analysis of Cracked Laminates, A Variational Approach", Mechanics of Materials, Vol. 4, p. 121, 1985.
8. Nairn, J.A., "The Strain Energy Release Rate of Composite Microcracking: A Variational Approach", J. Composite Materials, Vol. 23, p. 1009, 1989.
9. Chatterjee, S.N., "Damage Growth Modeling in Ceramic Matrix Composites", MSC TFR 3402/LD02, for Pratt & Whitney NASA EPM Program, April 1994.
10. Allen, D.H., Harris, C.E., and Graves, S.E., "A Thermo-Mechanical Constitutive Theory for Elastic Composites with Distributed Damage", International Journal of Solids and Structures, Parts I and II", Vol. 23, p. 1301, 1987.
11. Chatterjee, S.N., Teti, G., and Sasdelli, M., "Development of Design Software and Material Failure Models for Fiber Reinforced Plastic Pressure Hulls, Parts 1 and 2", MSC TFR 3401/1437 and 3502/1437, NSWC Contract N00167-93-C-0022, May 1994 and March 1995.
12. Kistner, M.D., Whitney, J.M., and Browning, C.R., "First-Ply Failure of Graphite/Epoxy Laminates", ASTM STP 864, pp. 44-61, 1985.

13. Illankamban, R., and Krajcinovic, D., "A Constitutive Theory for Progressively Deteriorating Solids", International Journal of Solids and Structures, Vol. 23, No. 11, p. 1521, 1987.
14. ____, "Advanced Technology Composite Aircraft Structures", Technical Progress Reports, NASA/Boeing ATCAS Program, Contract No. NAS1-1889, 20013, 1989-1995.
15. Chatterjee, S.N., Yen, C.F., Ramnath, V., and Wung, E.C.J., "Development of a 3-Dimensional Stress Analysis to Examine Static and Fatigue Fracture", MSC TFR 2118/1111, NAWC Contract No. N62269-87-C-0238, November, 1990.
16. Kessler, J., and Adams, D.F., "Standardization of Test Methods for Laminated Composites, Vol. II. Experimental Efforts, Appendix: Stress Strain Curves and Photographs", MSC TFR 3313/1706-002, U.S. Army Research Lab., Contract No. DAAL04-89-C-0023, October 1993.
17. Lagace, P.A., "Nonlinear Stress-Strain Behavior of Graphite/Epoxy Laminates", Proc. Part I.", AIAA/ASME/ASCE/AHS 25th Structures, Structural Dynamics and Materials Conference, AIAA, New York, p. 63, 1984.
18. Shuart, M.J., "Failure of Compression Loaded Multidirectional Composite Laminates", Proc. AIAA/ASME/ASCE/AHS 29th SDM Conference, AIAA Paper No. 88-2293, Williamsburg, VA, April 1988.
19. Whitney, J.M., and Nuismer, R.J., "Stress Fracture Criteria for Laminated Composites Containing Stress Concentrations", J. Composite Materials, Vol. 8, p. 253, 1974.
20. Awerbuch, J., and Madhukar, M., "Notched Strength of Composite Laminates: Predictions and Experiments - A Review", J. Reinforced Plastics and Composites, Vol. 4, p. 3, 1985.
21. Chatterjee, S.N., Yen, C.F., and Oplinger, D.W., "On the Determination of Tensile and Compressive Strengths of Unidirectional Fiber Composites", ASTM 6th Symposium on Composites: Fatigue and Fracture, Denver, CO, May 16-17, 1995, to appear in STP.

Table 1. Properties for a Carbon/Epoxy (AS/3501) Material

$E_1 = 18.85$ Msi, $E_2 = 1.52$ Msi, $\nu_{12} = 0.35$, $G_{12} = 0.87$ Msi

Values of a_{ij}, b_i

ϕ, lb/in^2	a_{11}	a_{22}	a_{33}	a_{12}	b_1	b_2
0	.5556E5	.9028E5	.4455E5	.4863E5	0	.3472E5
2.4	.2000E5	.3602E5	.2000E5	.1339E5	0	.1602E5
11.2	.1285E5	.1528E5	.8889E4	.4049E4	.1545E3	.8355E4
25.7	.1051E5	.8061E4	.5000E4	.2383E4	.2436E3	.3774E4
47.2	.9969E4	.5447E4	.3200E4	.1846E4	.4569E3	.2174E4
96.5	.9339E4	.2748E4	.1633E4	.1333E4	.4143E3	.2110E3
155.5	.8749E4	.1659E4	.9877E3	.8865E3	.3815E3	-.4089E3
300	.7620E4	.7620E3	.5203E3	.3485E3	.2913E3	-.5665E3
650	.6001E4	.3004E3	.2148E3	0	.3117E3	-.3004E3
950	.5009E4	.1566E3	.1533E2	0	.2503E3	-.1566E3
2000	.2871E4	.1028E-5	0	0	.6524E2	0
2800	.2036E4	0	0	0	.4545E2	0
3700	.1477E4	0	0	0	.2408E2	0
5500	.8556E3	0	0	0	-.5309E1	0
7500	.5174E3	0	0	0	-.2907E2	0

Note: For numerical calculations, the zero values for a_{22} and a_{33} listed at the end of the table are chosen as very small numbers decreasing with increasing ϕ.

Table 2. Integrated Values of Coefficients

$$A_{ij}, B_i = \int_0^{\phi} (a_{ij}, b_i) d\phi$$

Units of all quantities = lb/in^2

ϕ	A_{11}	A_{22}	A_{33}	A_{12}	B_1	B_2
0	0	0	0	0	0	0
2.4	.9067E5	.1516E6	.7746E5	.7443E5	0	.6088E5
11.2	.2352E6	.3772E6	.2046E6	.1512E6	.6800E3	.1681E6
25.7	.4046E6	.5464E6	.3053E6	.1978E6	.3566E4	.2560E6
47.2	.6247E6	.6916E6	.3934E6	.2433E6	.1110E5	.3200E6
96.5	.1101E7	.8936E6	.5125E6	.3216E6	.3257E5	.3788E6
155.5	.1634E7	.1024E6	.5898E6	.3871E6	.5605E5	.3729E6
300	.2817E7	.1199E7	.6988E6	.4763E6	.1047E6	.3025E6
650	.5201E7	.1384E7	.8274E6	.5373E6	.2102E6	.1508E6
950	.6852E7	.1453E7	.8619E6	"	.2945E6	.8221E5
2000	.1099E8	.1535E7	.87E6	"	.4602E6	0
2800	.1295E8	"	"	"	.5044E6	"
3700	.1453E8	"	"	"	.5357E6	"
5500	.1663E8	"	"	"	.5526E6	"
7500	.1801E8	"	"	"	.5183E6	"
Limit	.1904E8	.1535E7	.87E6	.5373E6	0	0

Table 3. Maximum Values of Computed Dissipated Energy Densities in Each Layer of $(\pm\theta)_{ns}$ Coupons

Layup	Max. Axial Strain %	Maximum ϕ, lb/in^2
$(\pm 45)_{ns}$ Tension	1.2	35
$(\pm 45)_{ns}$ Tension	5.0*	664
$(\pm 50)_s$ Tension	1.5	49
$(\pm 30)_s$ Tension	1.4	121
$(\pm 60)_{ns}$ Compression	2.5	101
$(\pm 30)_{ns}$ Compression	0.95	70
$(\pm 20)_{ns}$ Compression	1.0	168

* This strain level is too high and corresponds to about 10% shear strain for which geometry changes will play an important role.

Table 4. Figure Numbers for Tension Coupons with Hole

Laminate	Hole Dia.	Load-Deflection	SED in Various Layers
$(0/\pm 45/90)_s$	1/4"	Figure 18	Figures 19 - 22
	1/8"	Figure 23	Figures 24 - 27
$(0/\pm 60)_s$	1/4"	Figure 28	Figures 29 - 31
	1/8"	Figure 32	Figures 33 - 35

Table 5.

Laminate	Hole Diameter	Maximum Gross Stress σ_N ksi	σ_N/σ_o
$(0/\pm45/90)_s$	1/4"	58.0	0.592
	1/8"	66.0	0.673
	0	98* (σ_o)	1
$(0/\pm60)_s$	1/4"	49.3	0.509
	1/8"	54.7	0.565
	0	96.8* (σ_o)	1

* From single element results discussed in Task 2.

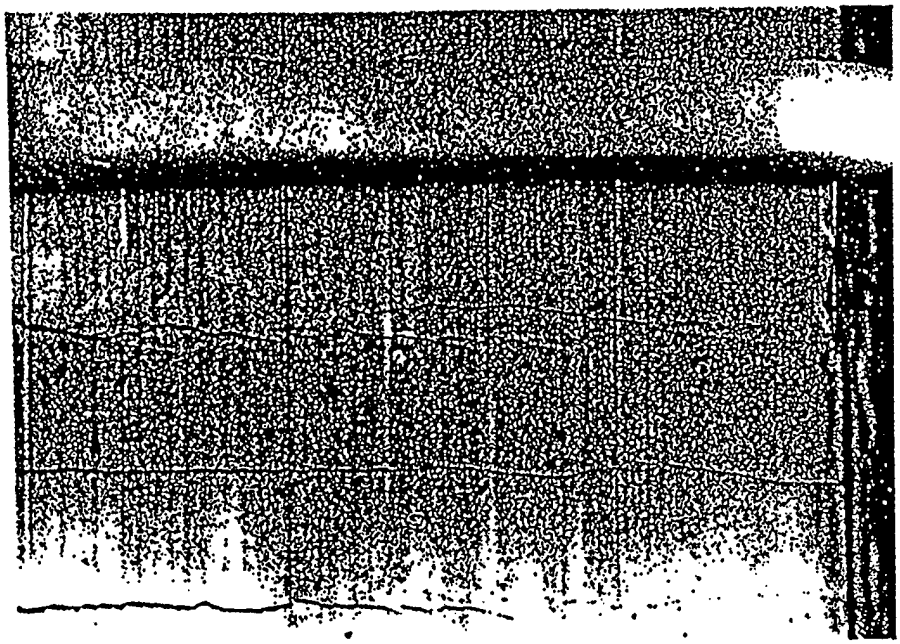

e) STRESS = 34.9 ksi
MACHINE STRAIN ≈ 1.46%

0.025 in.

Figure 1. Transverse Cracks in a Crossply $(0/90)_{ns}$ Laminate, Static Tension

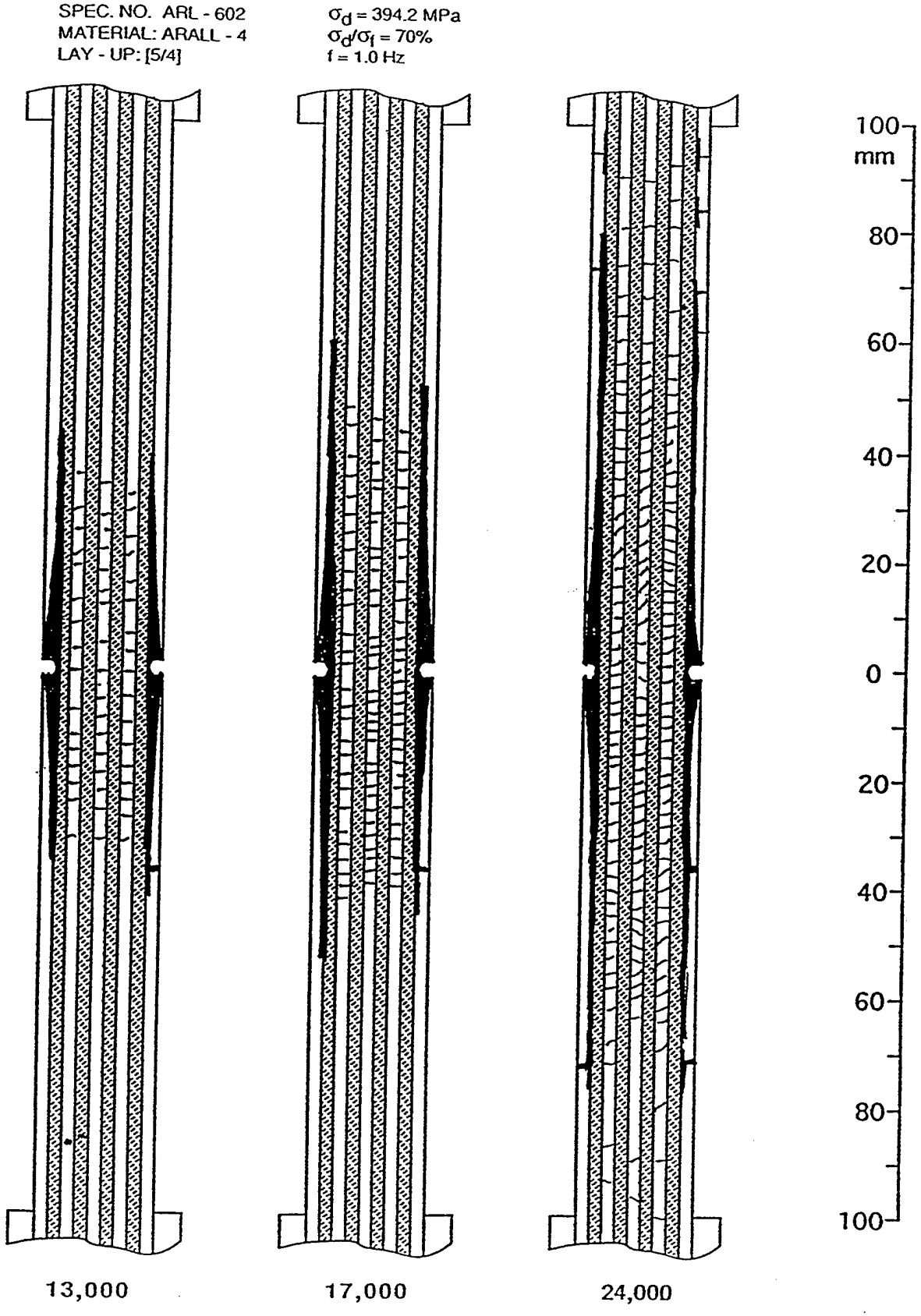

Figure 2. Closely Spaced Transverse Cracks and Delaminations Near a Stress Concentration, Tension-Tension Fatigue

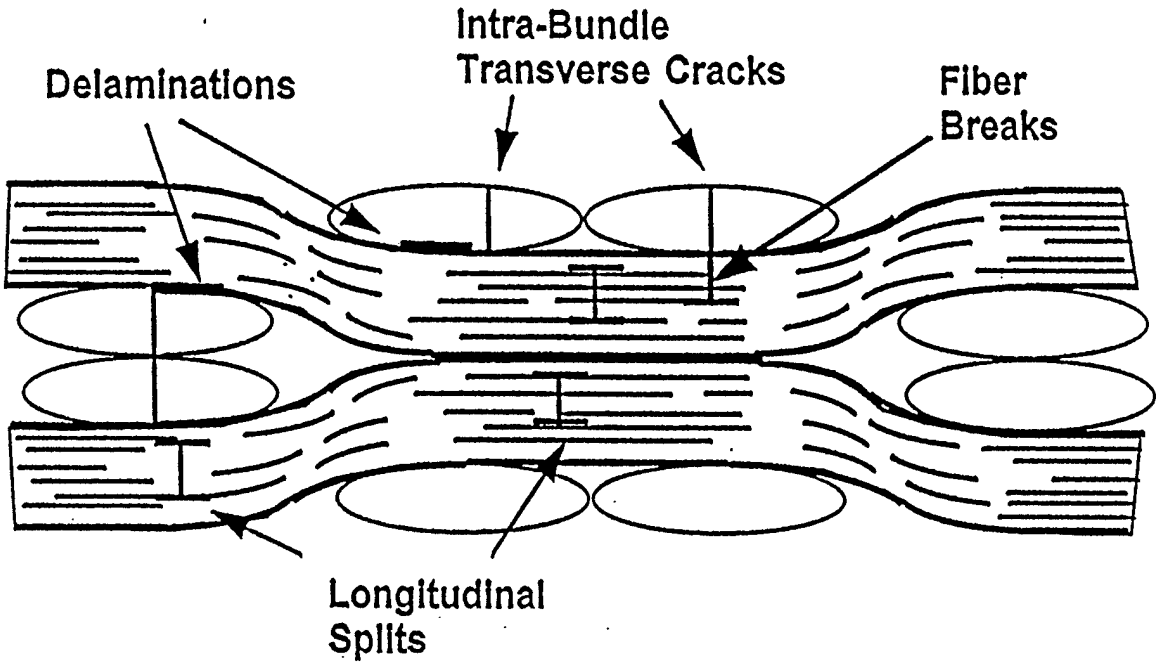

Figure 3. Various Damages, Schematic

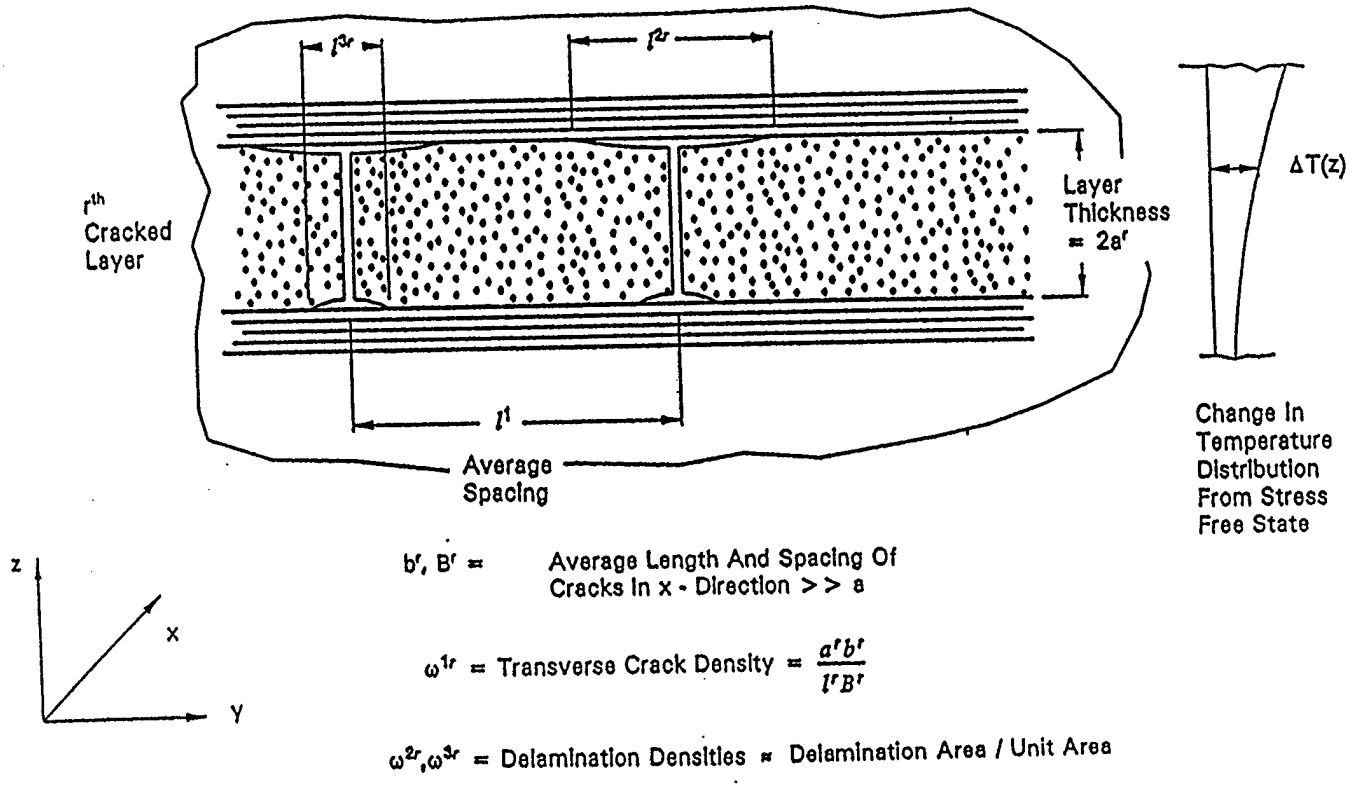

Figure 4. Transverse Cracks and Delaminations, Schematic

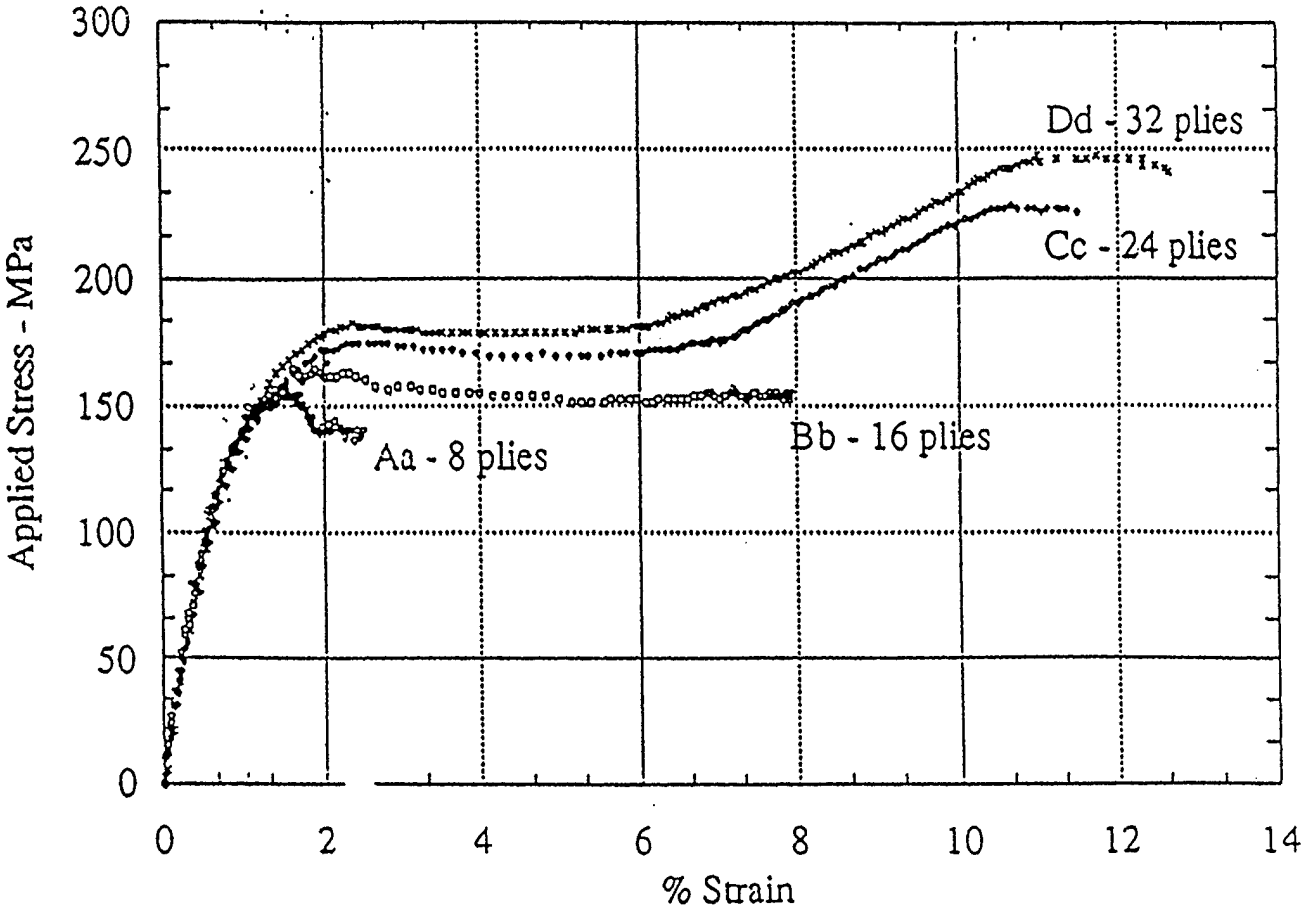

Figure 5. Average Axial Stress-Strain Response of $(\pm 45)_{ns}$ Laminates Under Static Tension

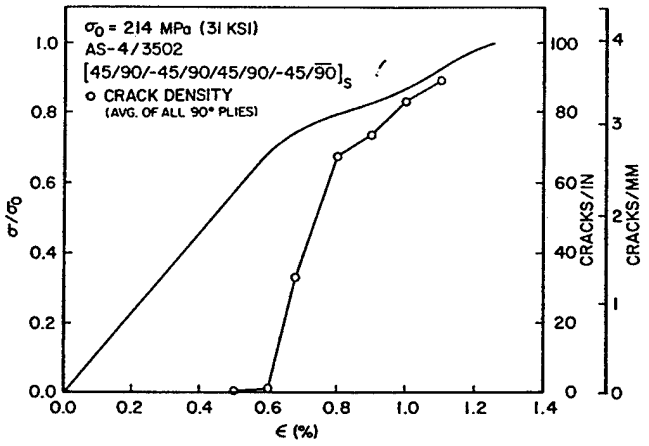

Figure 6a. Stress-Strain Response of [45/90/-45/90/45/90/-45/90]$_s$ Graphite/Epoxy Showing the Knee [12]

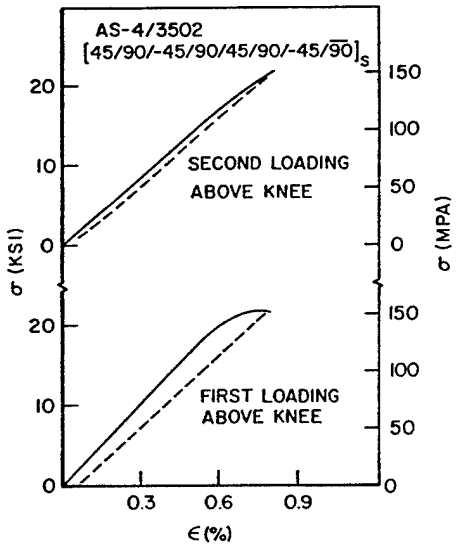

Figure 6b. First and Second Loading Above the Knee in the Stress-Strain Curve for [45/90/-45/90/45/90/-45/90]$_s$ Graphite/Epoxy [12]

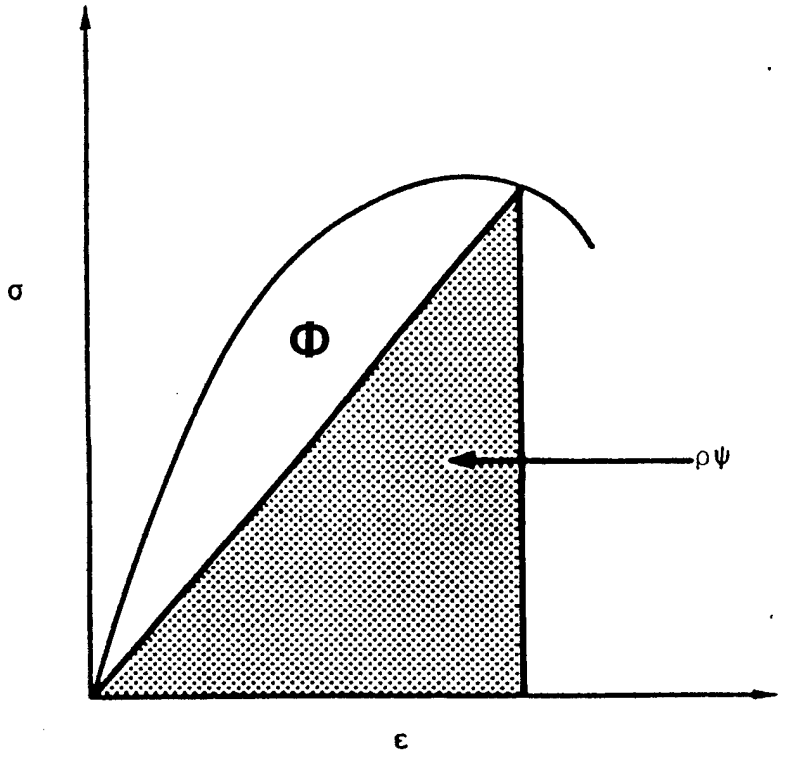

Figure 7. Helmholtz Free Energy $\rho\psi$ and Dissipated Energy ϕ

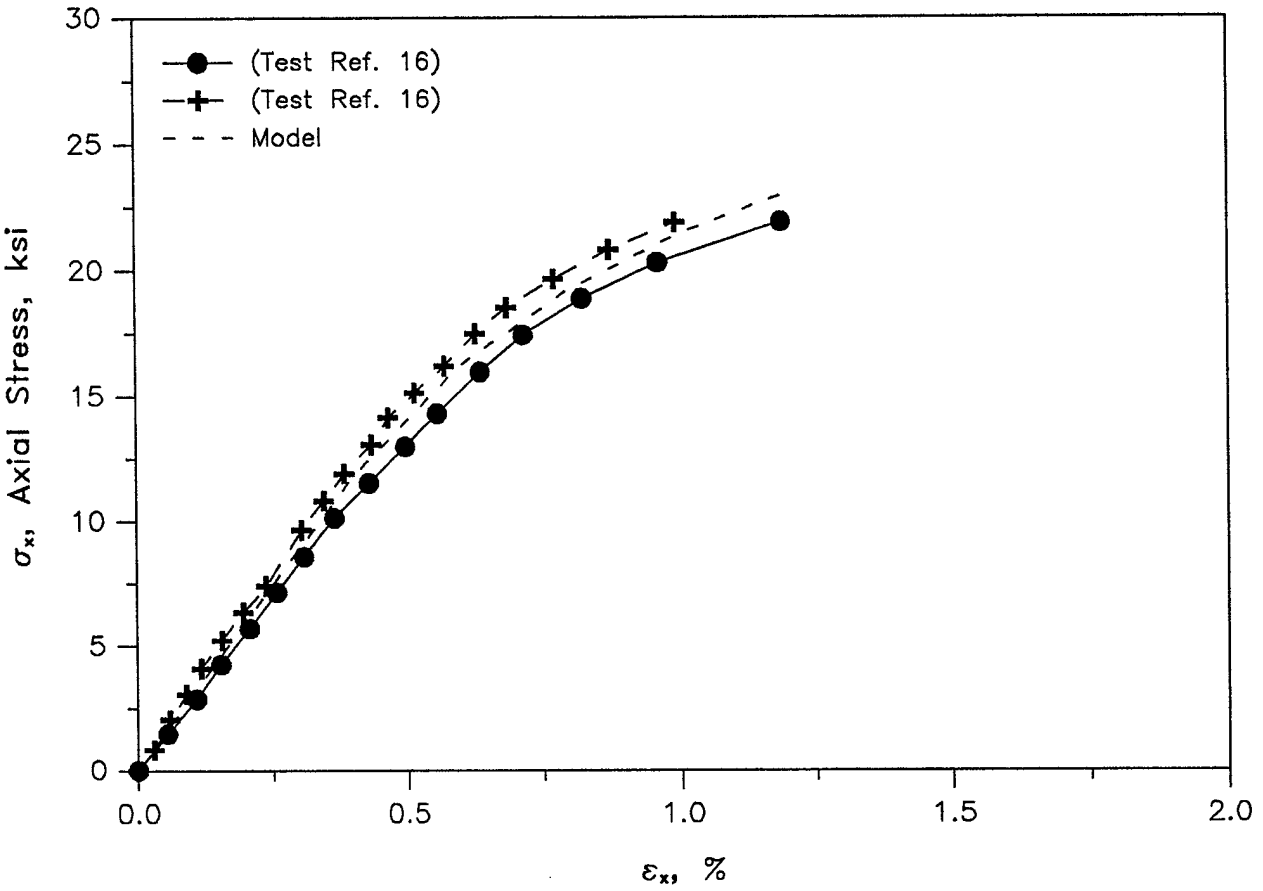

Figure 8a. Axial Stress vs. Axial Strain For $(\pm 45)_{ns}$ Tension.

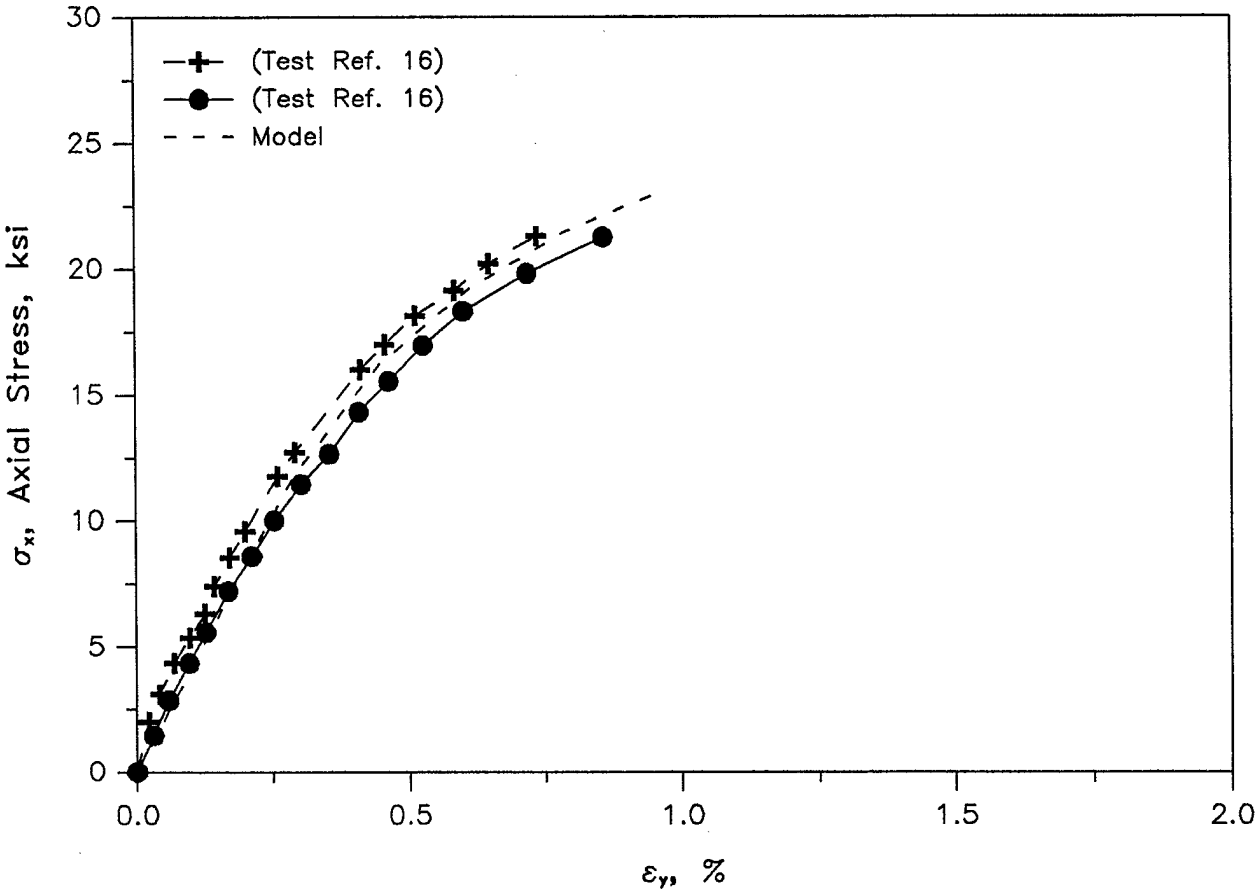

Figure 8b. Axial Stress vs. Transverse Strain For $(\pm 45)_{ns}$ Tension.

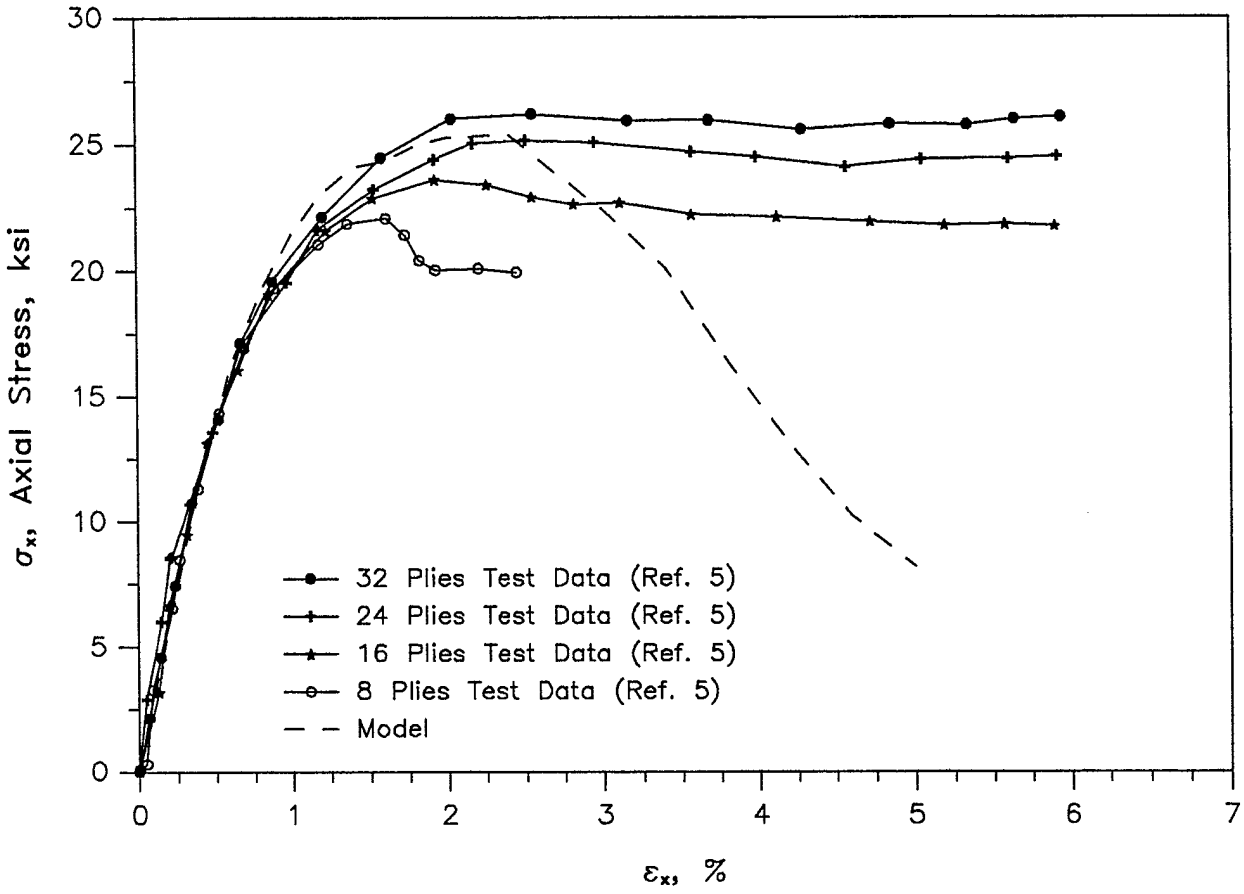

Figure 9. Axial Stress vs. Axial Strain For $(\pm 45)_{ns}$ Tension Up–To High Strain Levels

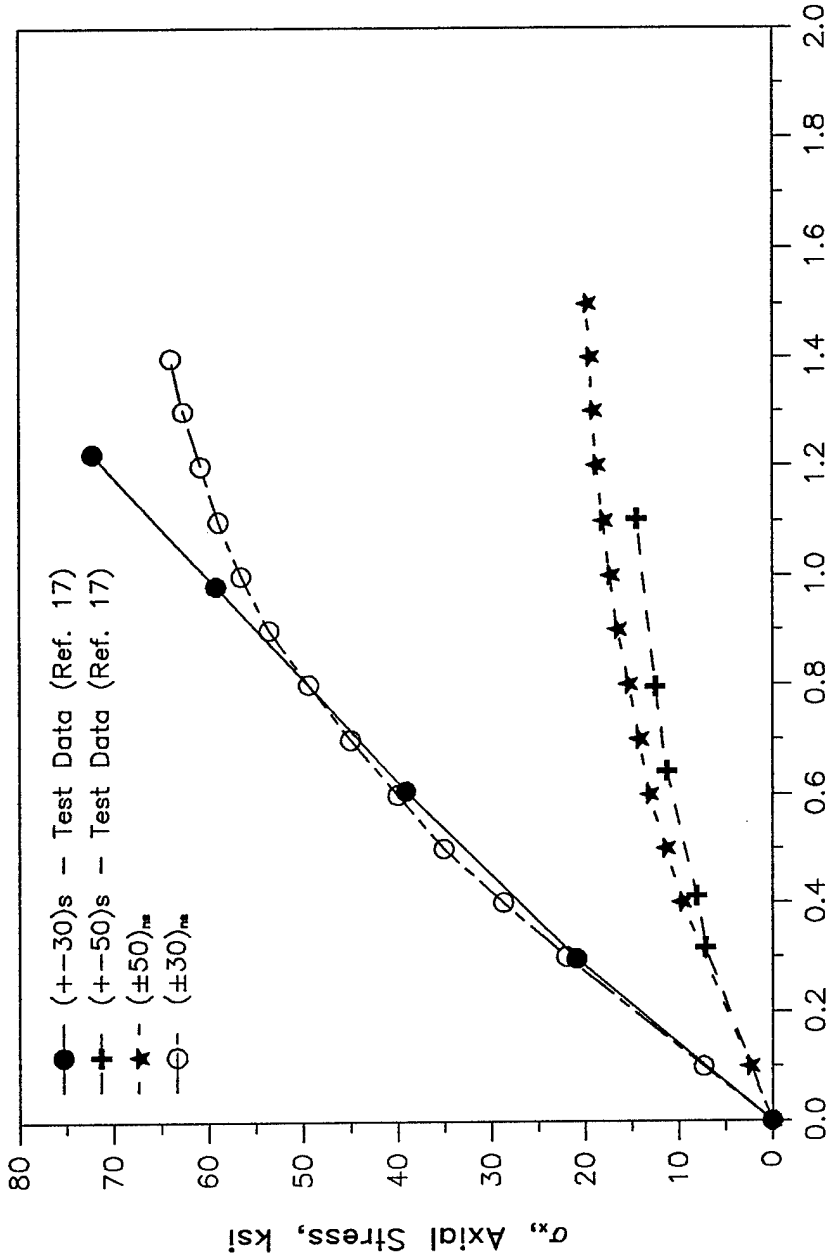

Figure 10. Axial Stress vs. Axial Strain For $(\pm 50)_{ns}$ And $(\pm 30)_{ns}$ Tension.

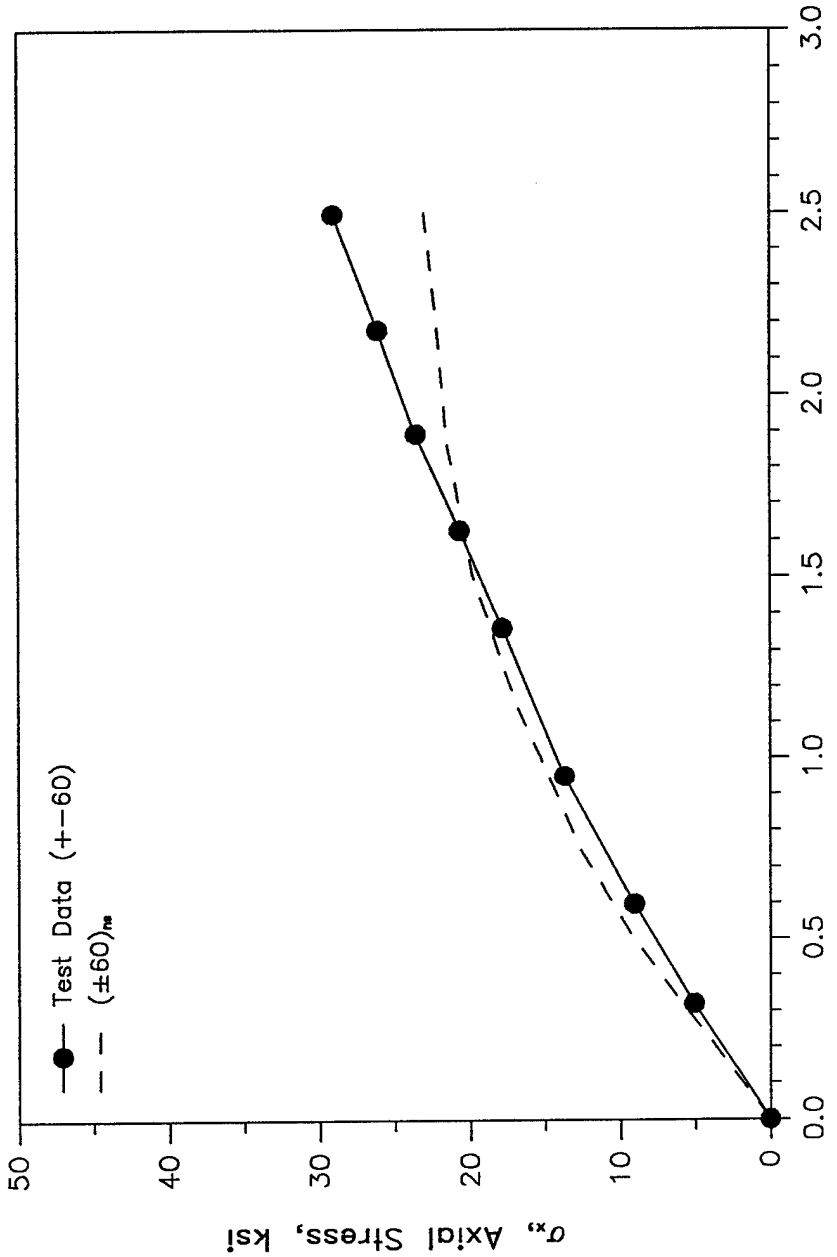

Figure 11. Axial Stress vs. Axial Strain For $(\pm 60)_{ns}$ Compression.

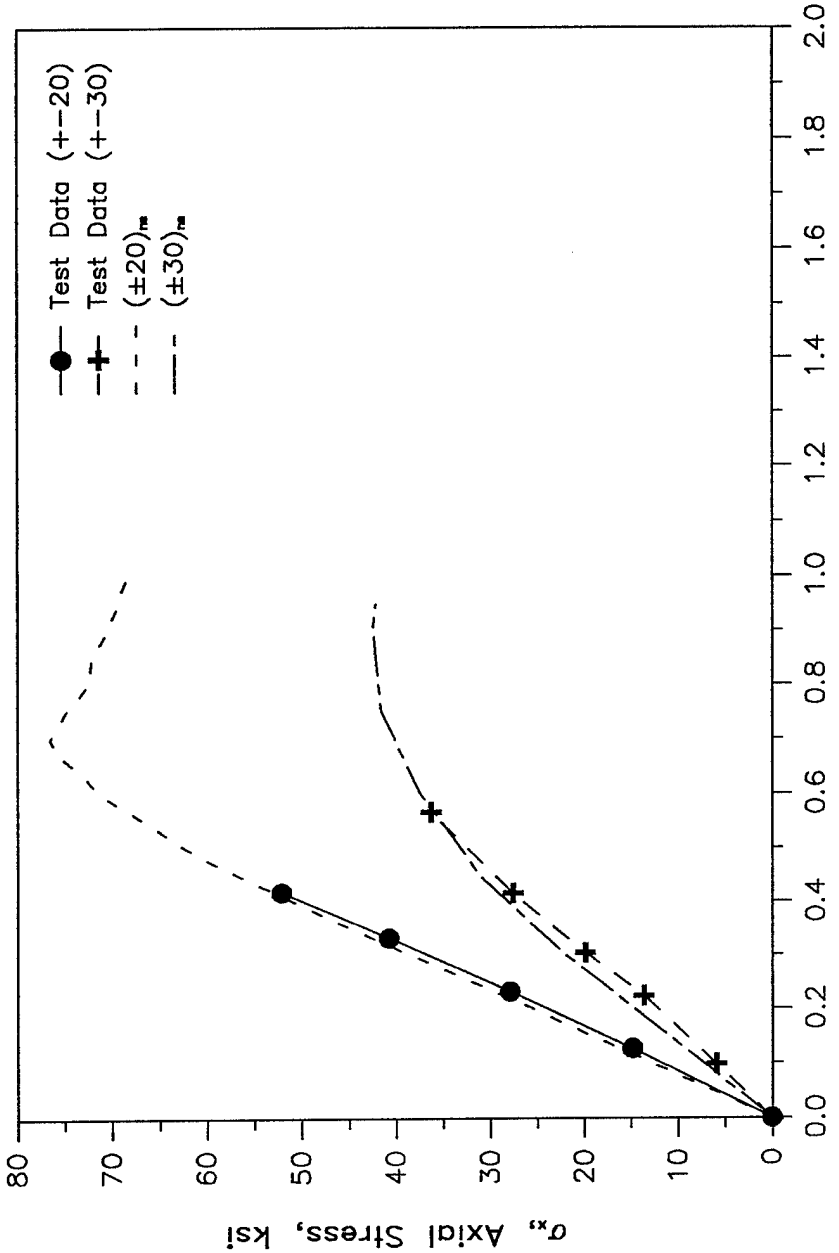

Figure 12. Axial Stress vs. Axial Strain For $(\pm 30)_{ns}$ And $(\pm 20)_{ns}$ Compression.

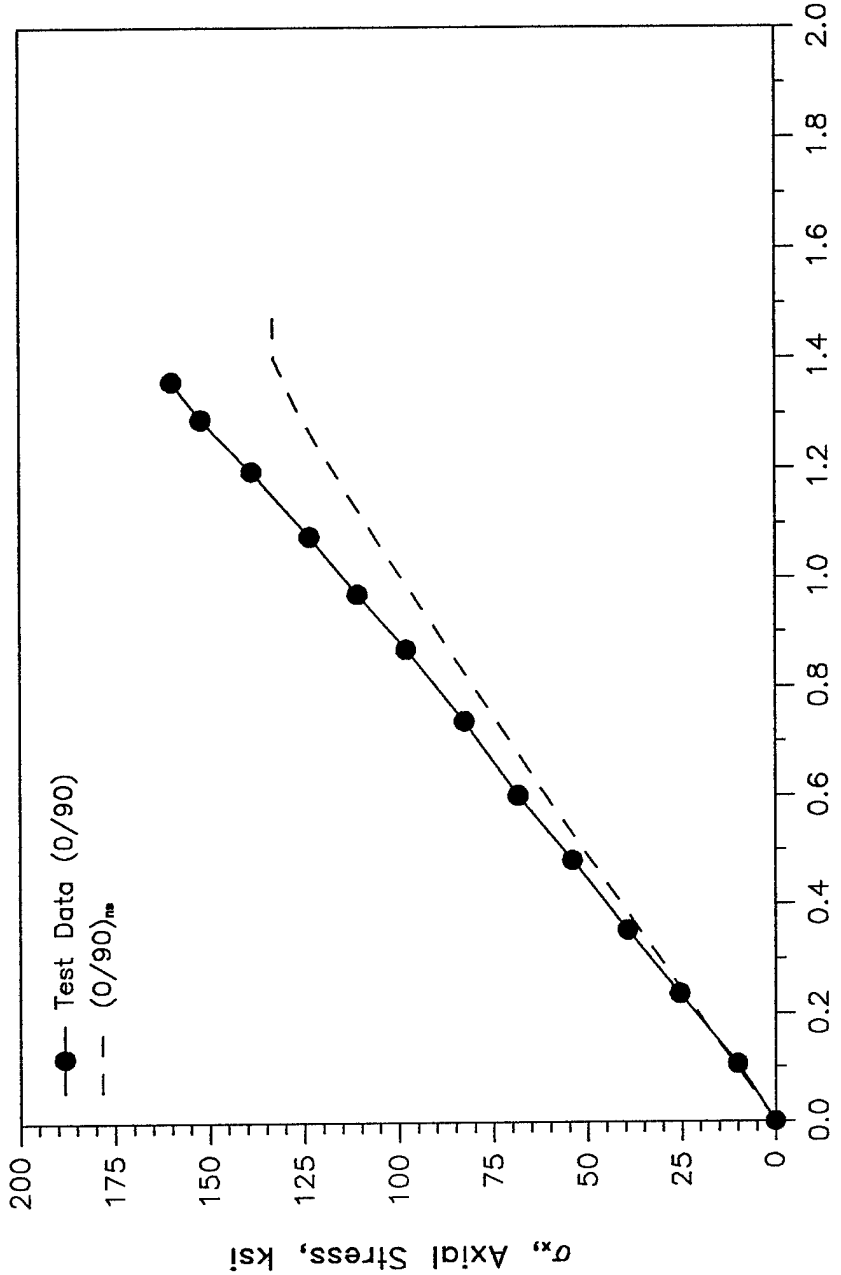

Figure 13a. Axial Stress vs. Axial Strain For $(0/90)_{ms}$ Tension.

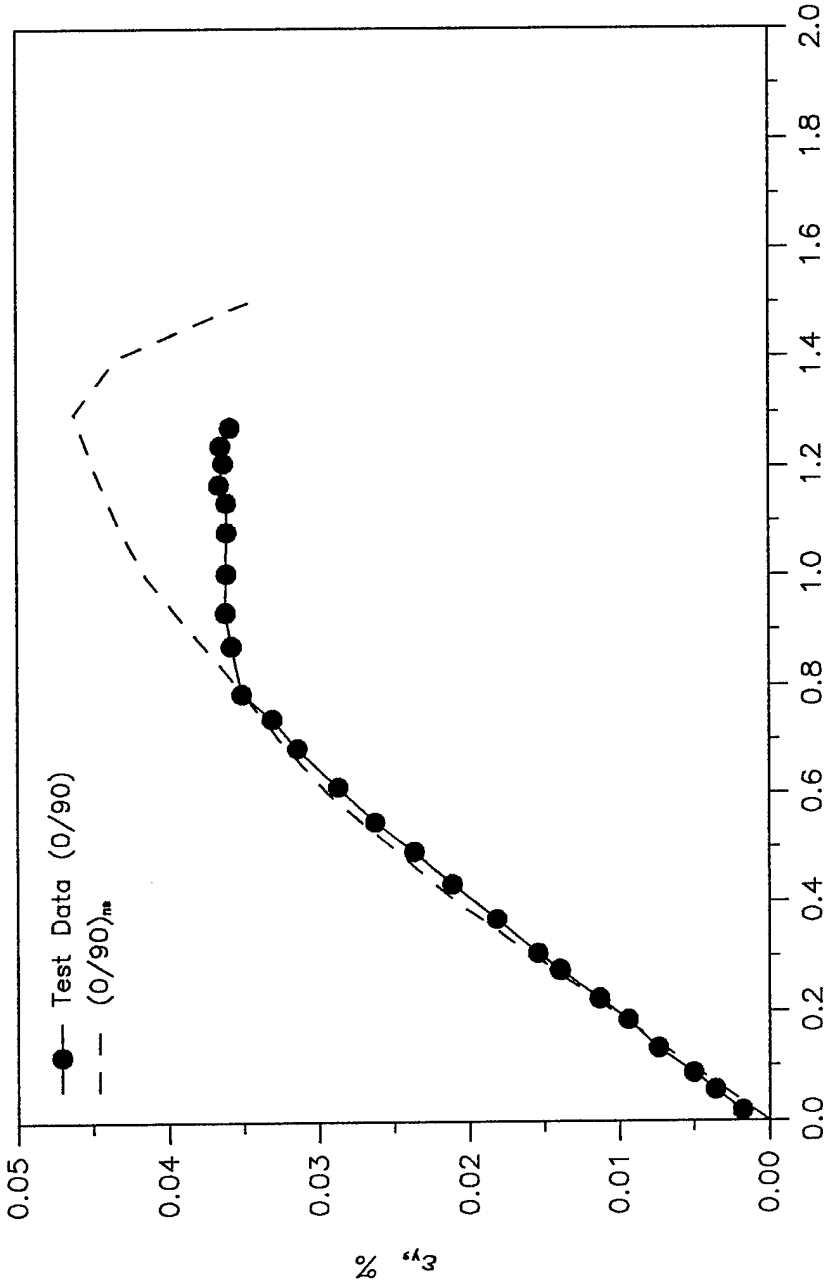

Figure 13b. Transverse Strain vs. Axial Strain For $(0/90)_{ns}$ Tension.

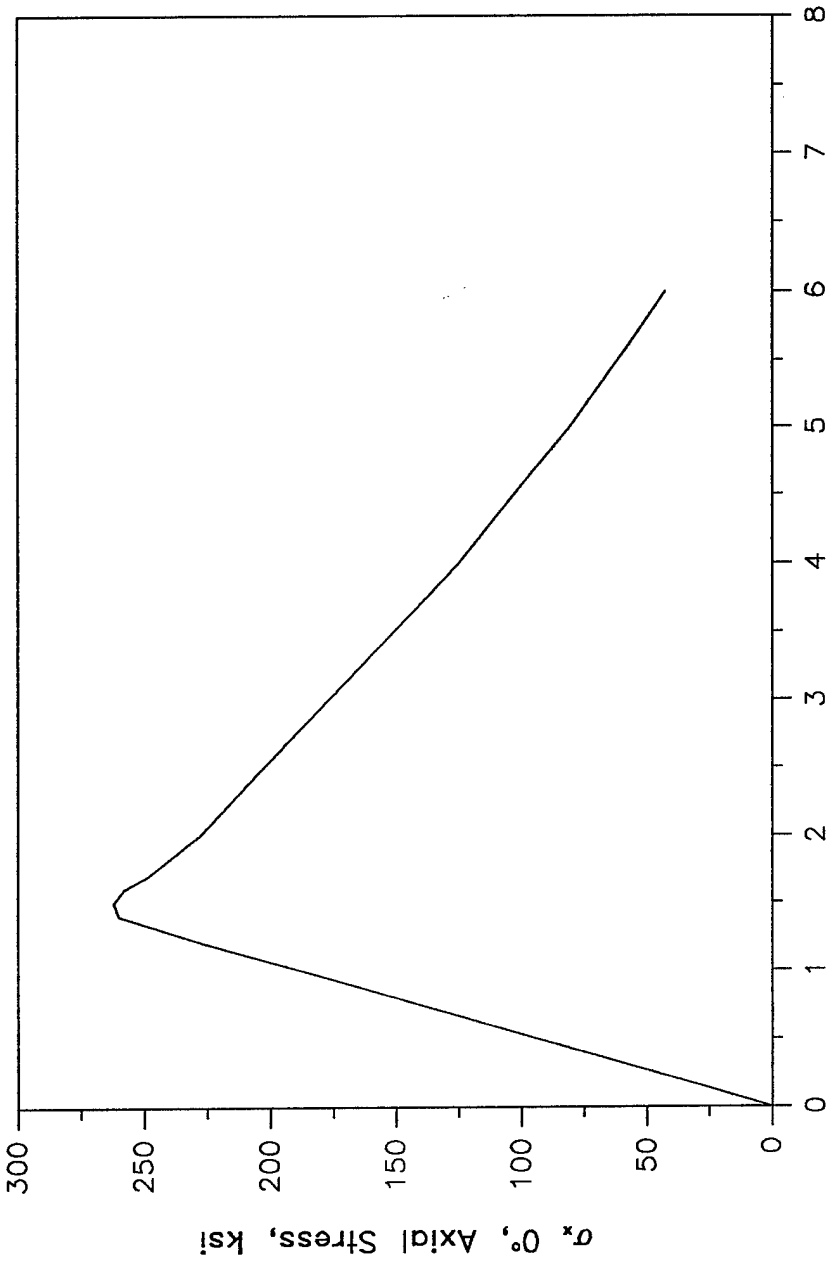

Figure 14. 0° Fiber Direction Stress vs Axial Strain For $(0/\pm45/90)_{ns}$ Tension.

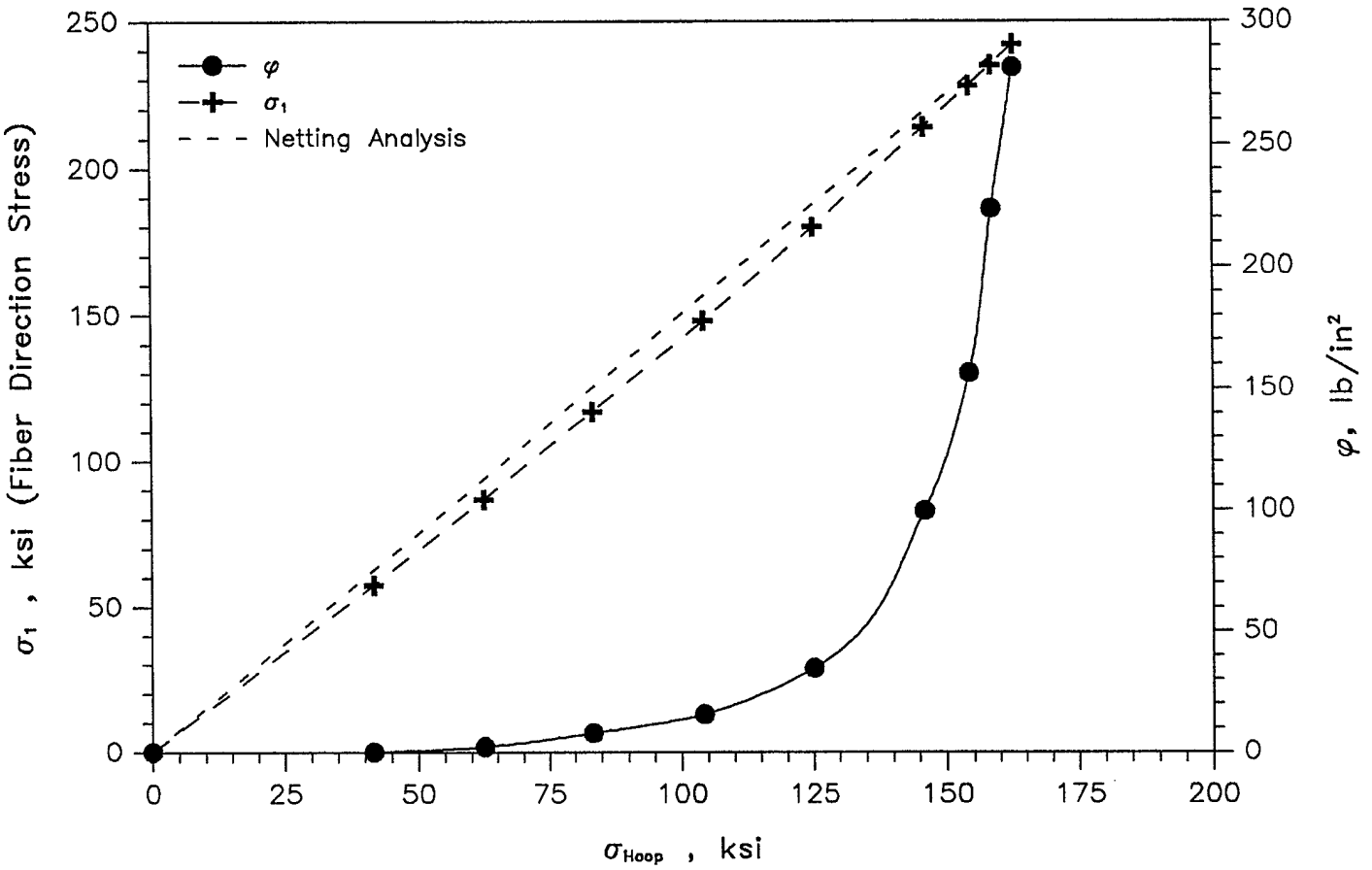

Figure 15a. Fiber Direction Stress σ_1 And DED φ In Each Layer Of A $(\pm 54.74°)_{ns}$ Pressure Vessel.

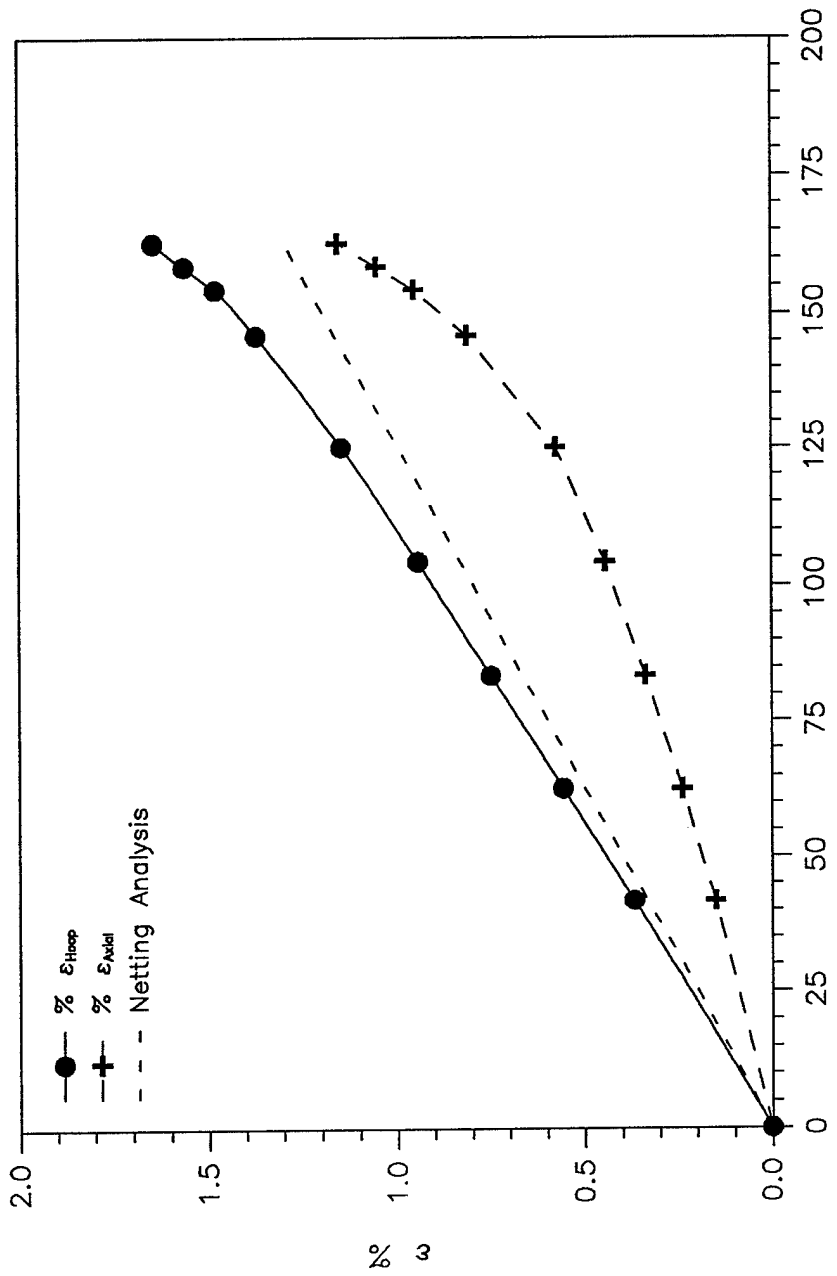

Figure 15b. Hoop And Axial Strains vs. Hoop Tensile Stress In A $(\pm 54.74^{\circ})_{ns}$ Pressure Vessel.

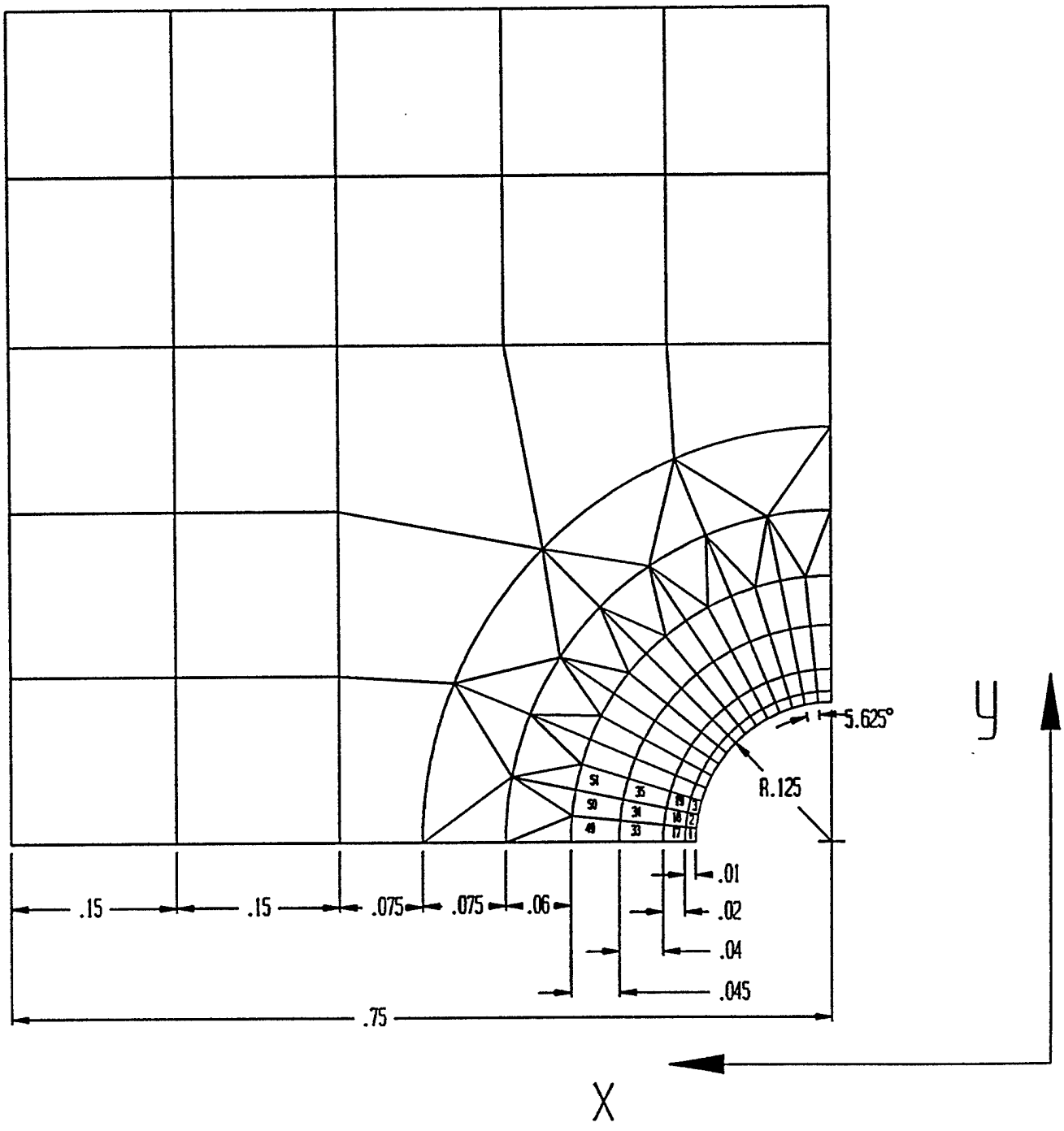

Figure 16. Finite Element Mesh Near A 0.25" Dia. Hole.

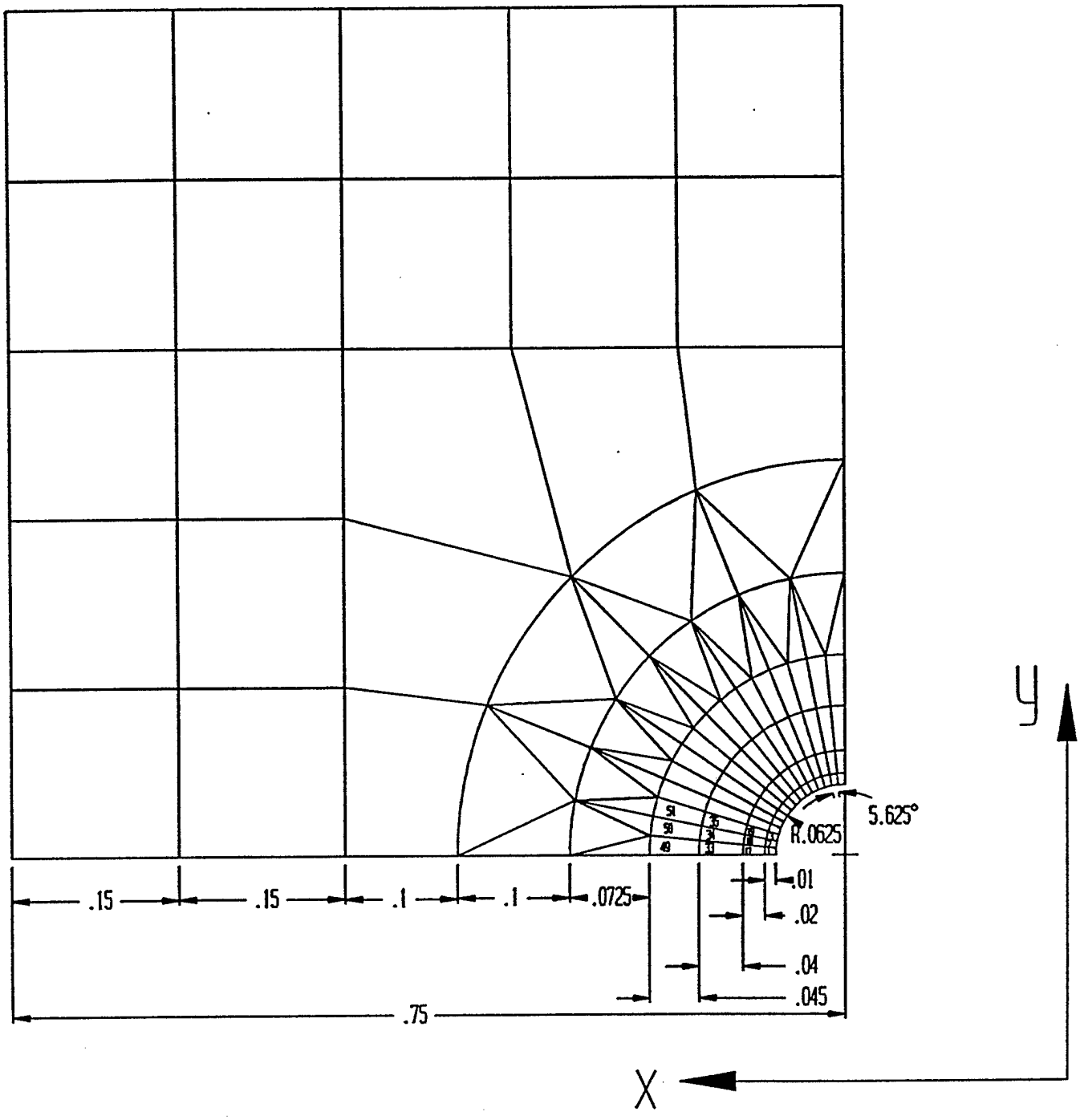

Figure 17. Finite Element Mesh Near A 0.125" Dia. Hole.

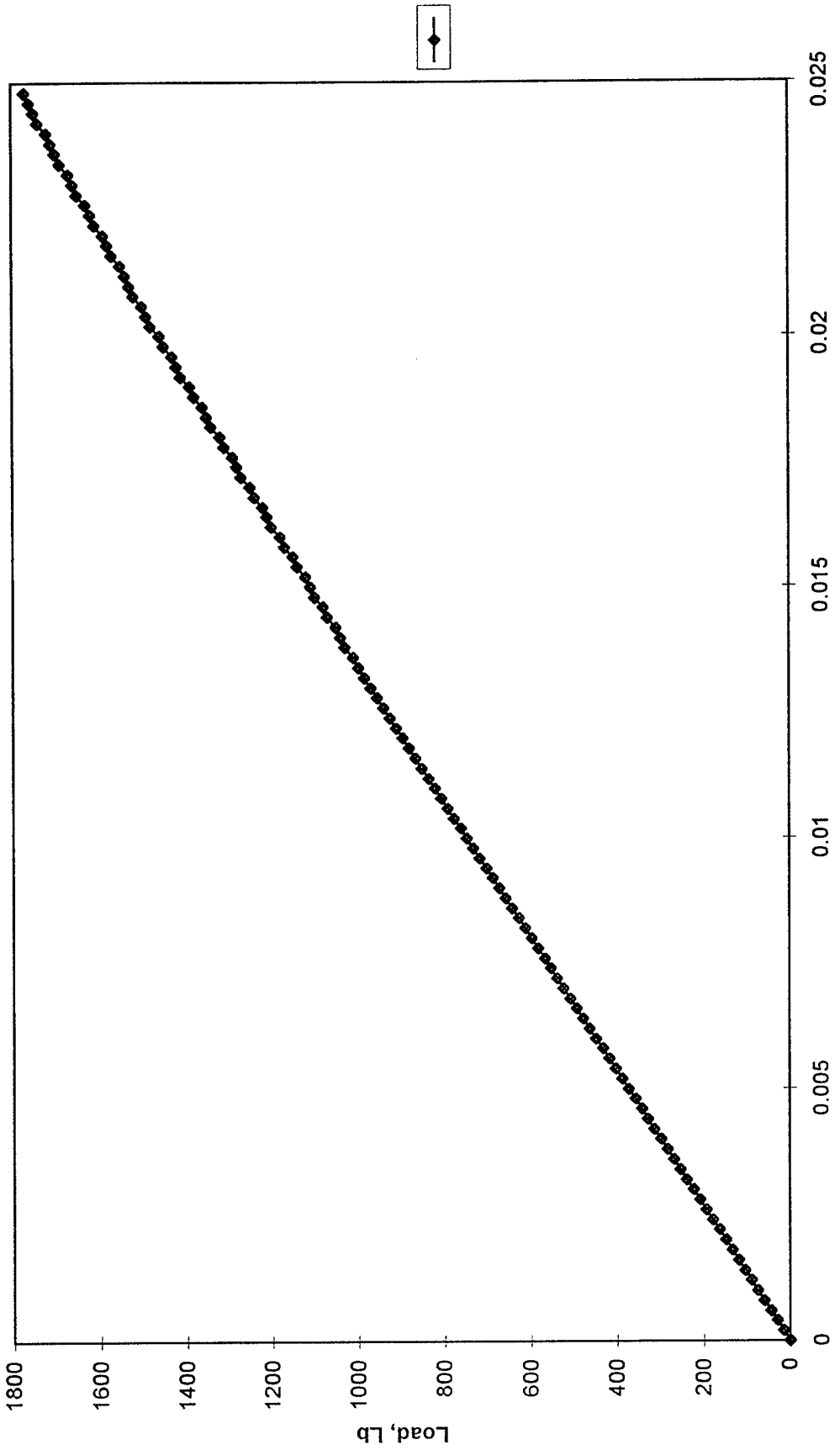

Figure 18. Load-Displacement Relation for [0/45/-45/90]s with a 1/4" Hole.

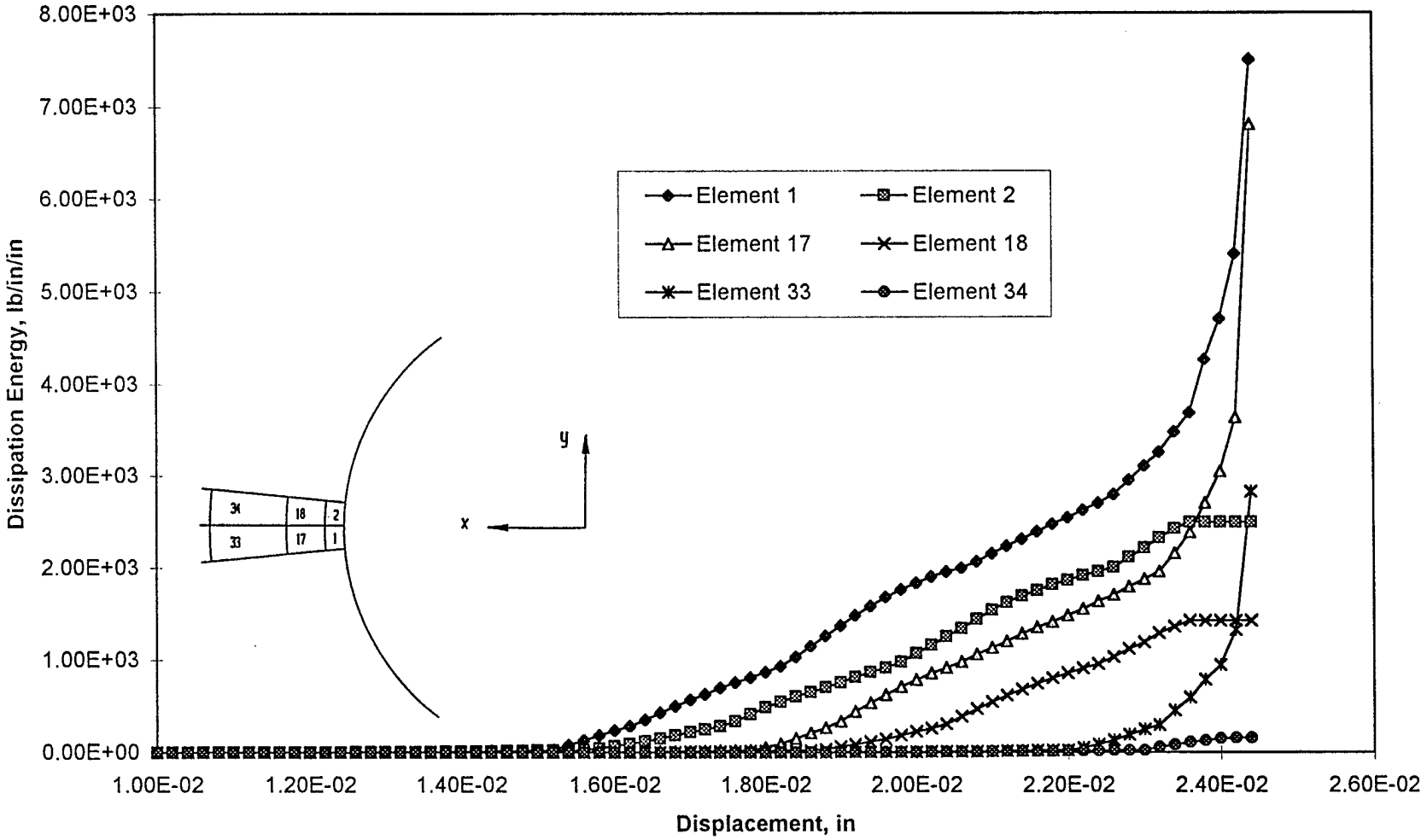

Figure 19. Dissipation Energy vs. Displacement for [0/45/-45/90]s with a 1/4" Hole, 0-Layer.

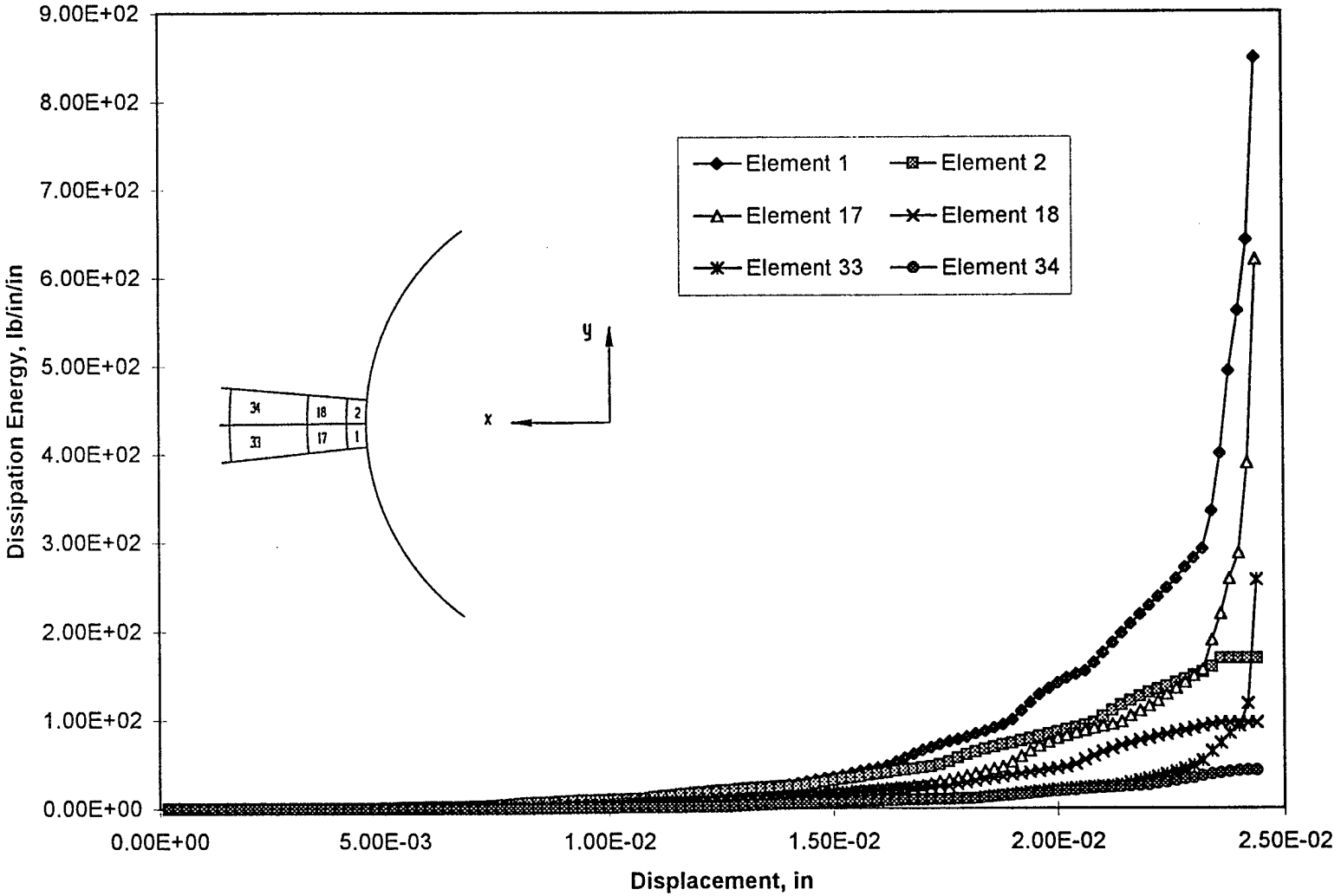

Figure 20. Dissipation Energy vs. Displacement [0/45/-45/90]s with a 1/4" Hole, 45-Layer.

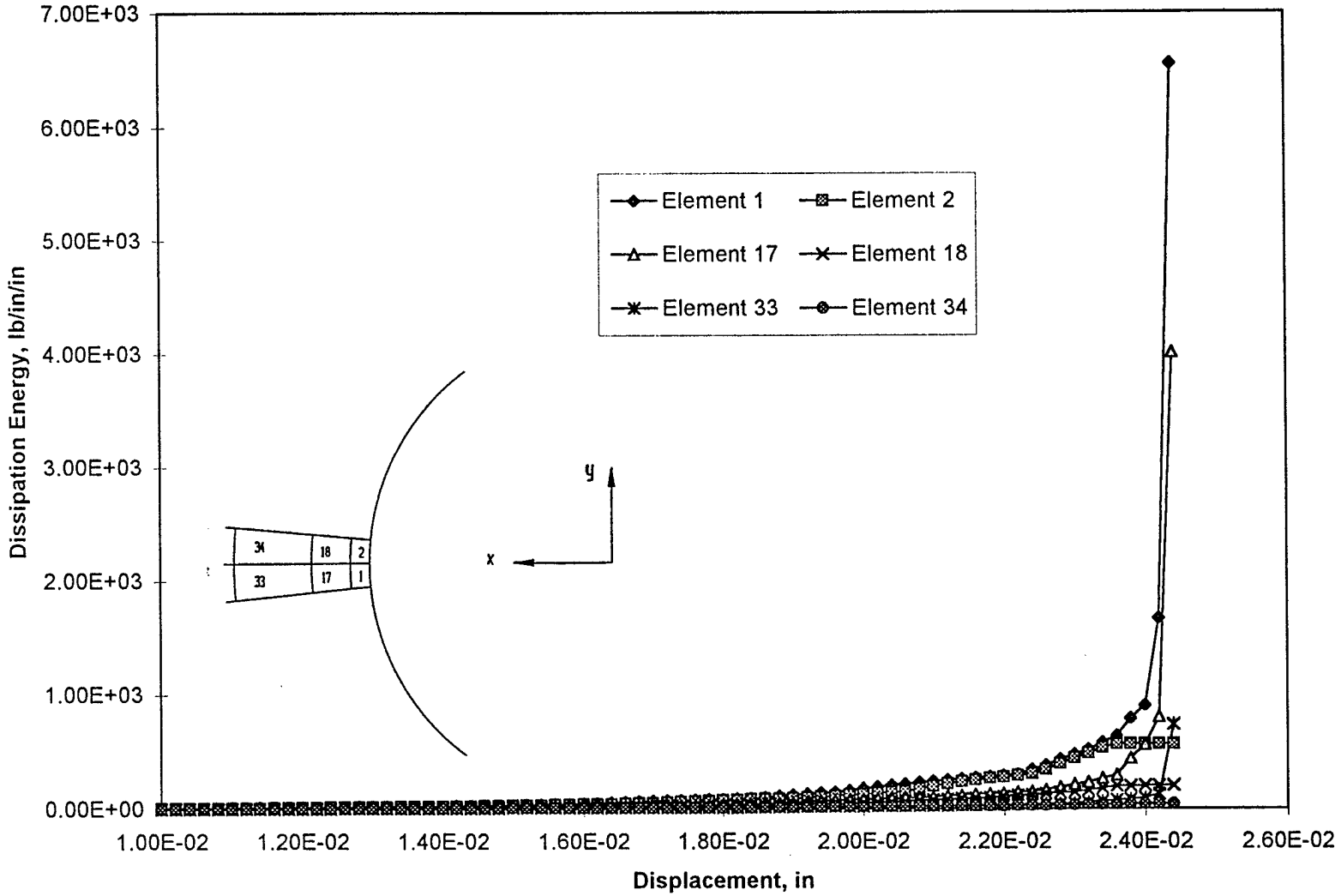

Figure 21. Dissipation Energy vs. Displacement for [0/45/-45/90]s with a 0.25" Hole, -45-Layer.

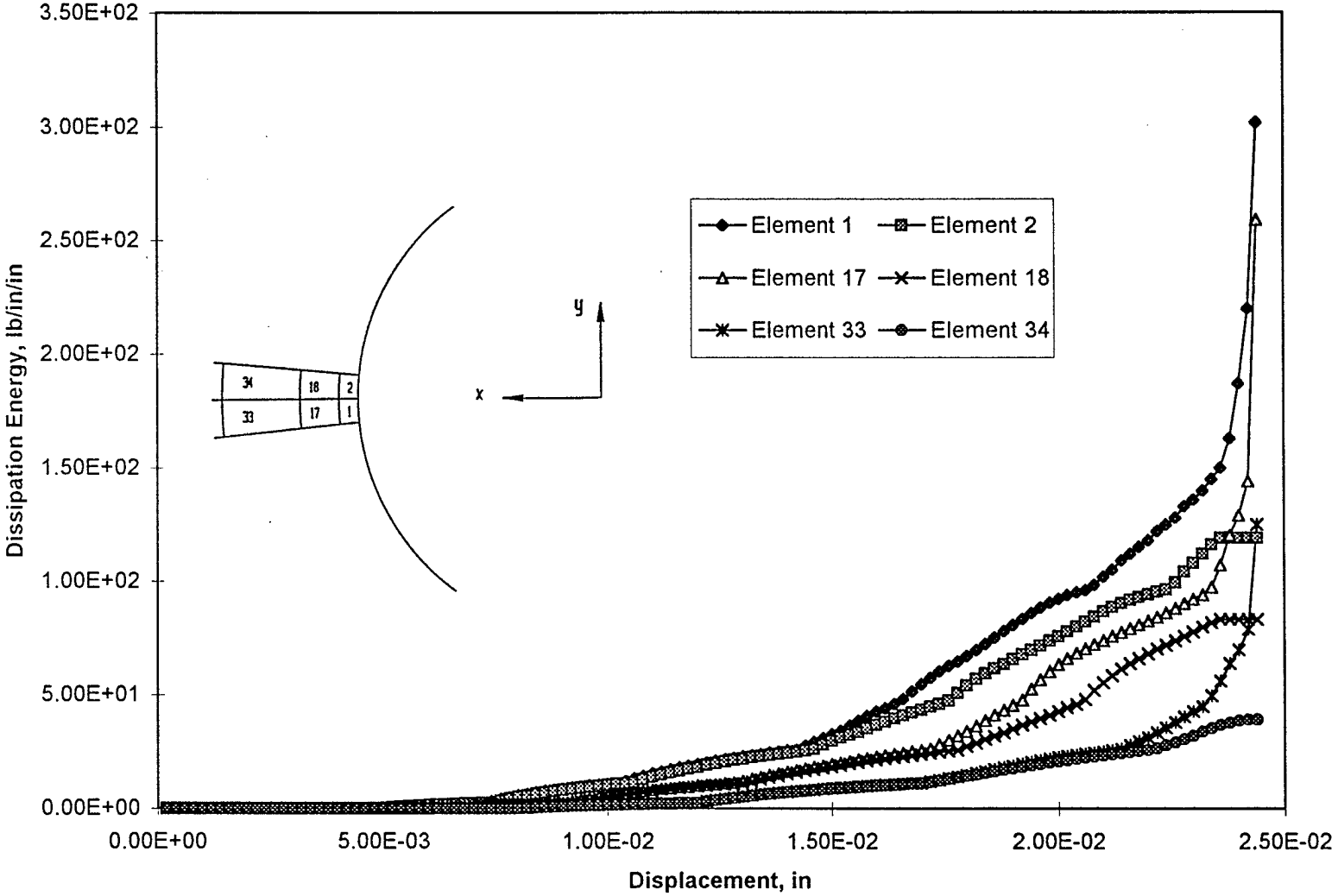

Figure 22. Dissipaation Energy vs. Displacement for [0/45/-45/90]s with a 1/4" Hole, 90-Layer.

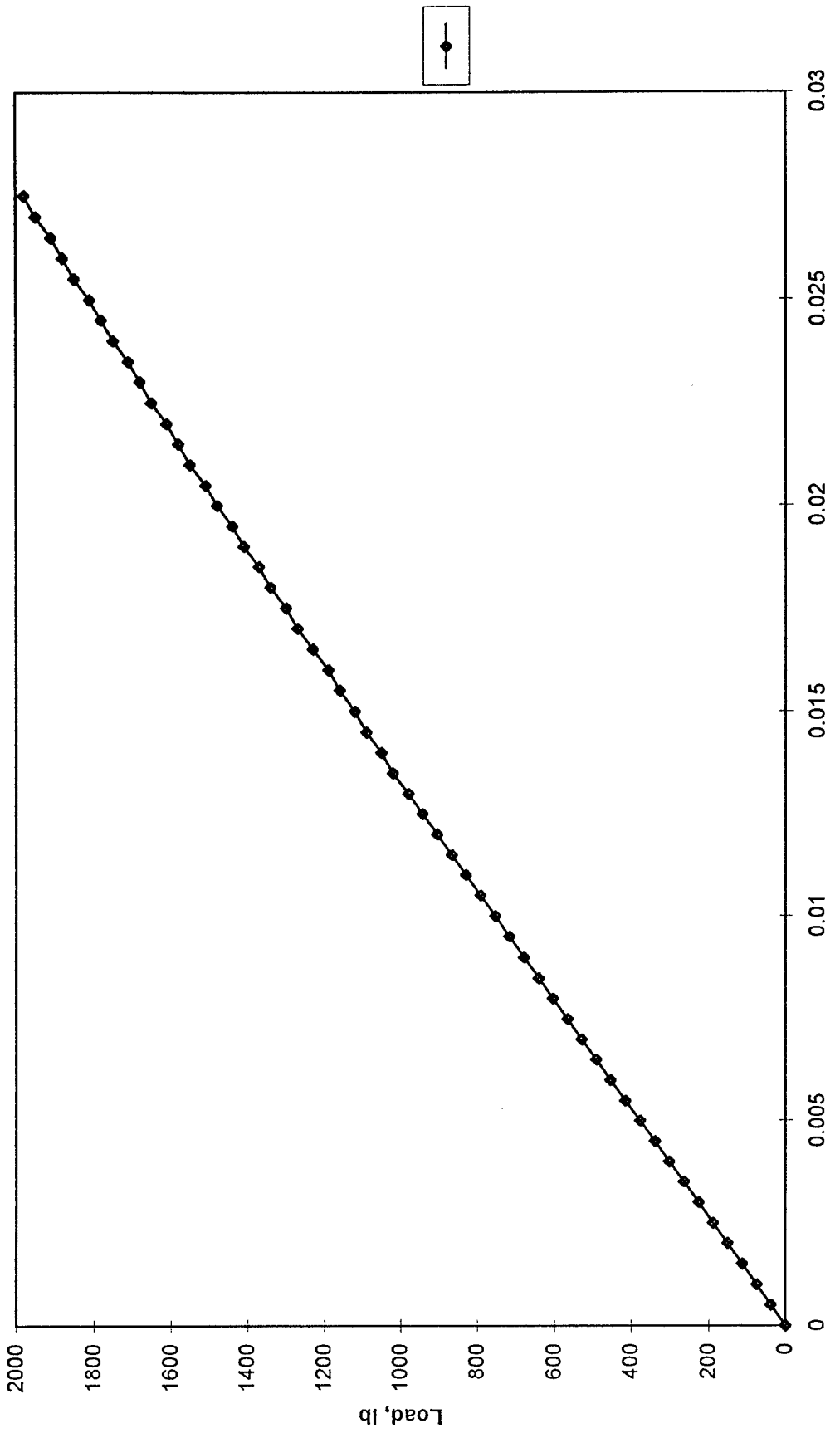

Figure 23. Load-Displacement Relation for [0/45/-45/90]s with a 1/8" Hole.

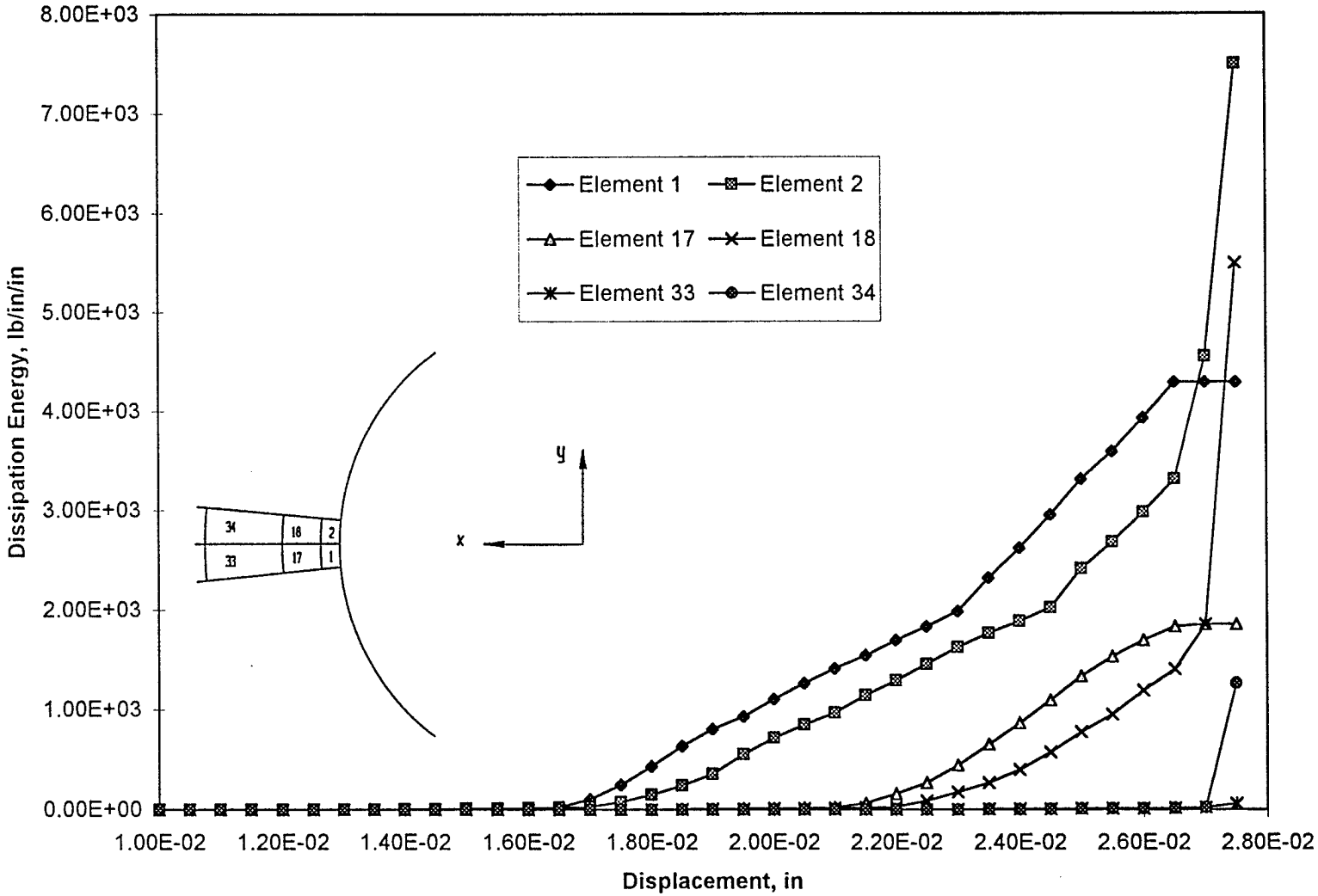

Figure 24. Dissipation Energy vs. Displacement for [0/45/-45/90]s with a 1/8" Hole, 0-Layer.

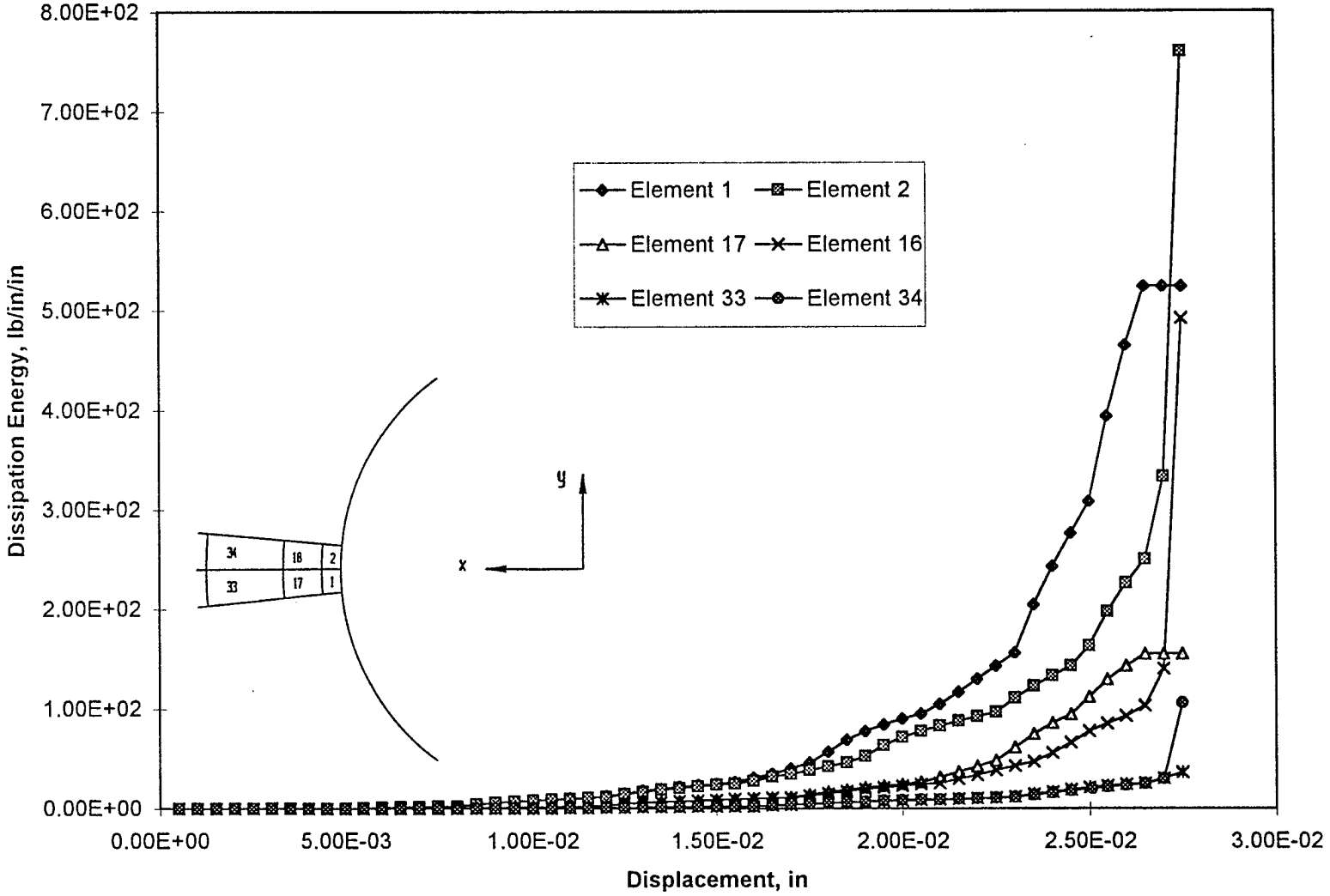

Figure 25. Dissipaation Energy vs. Displacement for [0/45/-45/90]s with a 1/8" Hole, 45-Layer.

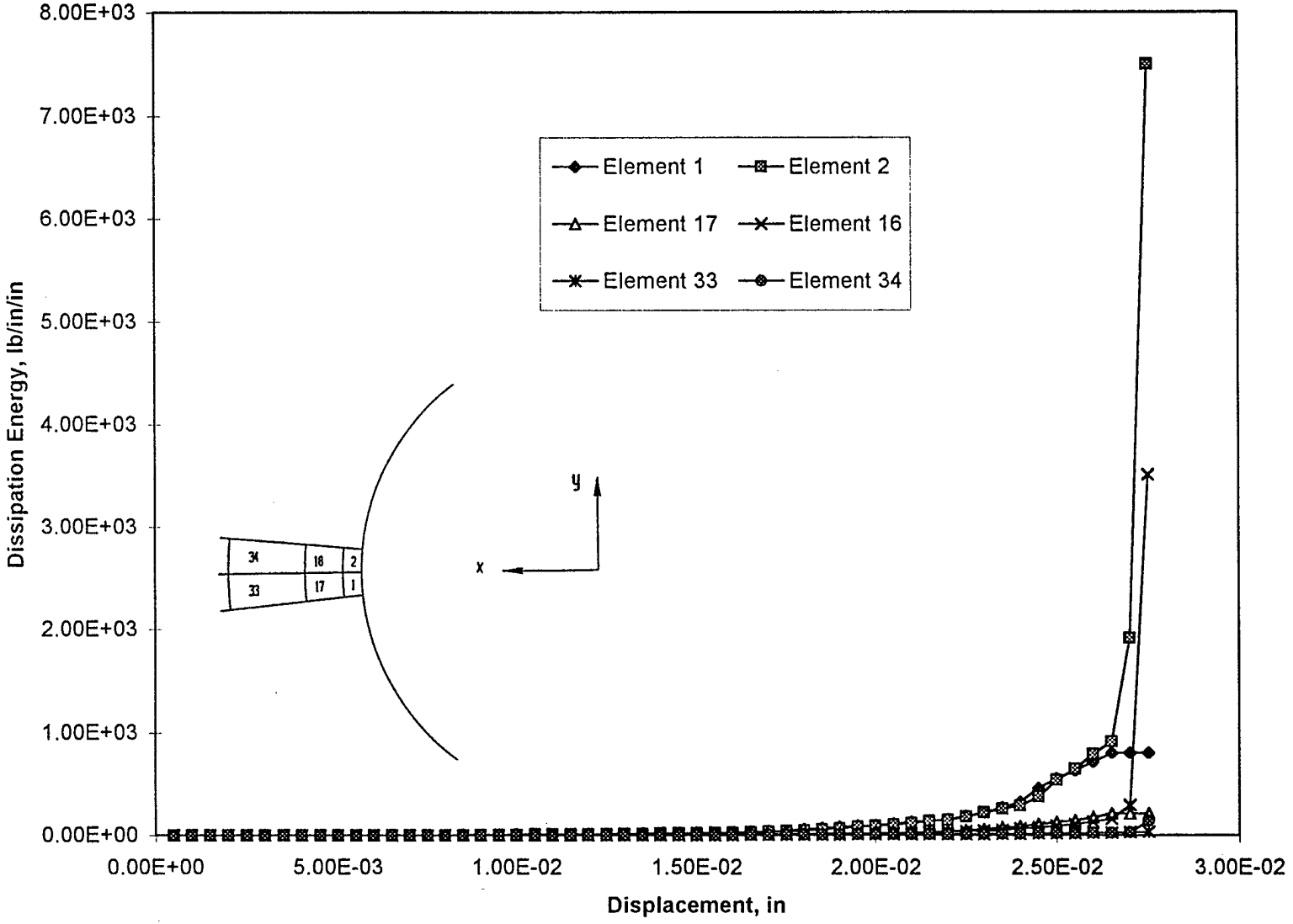

Figure 26. Dissipation Energy vs. Displacement for [0/45/-45/90]s with a 1/8" Hole, -45-Layer.

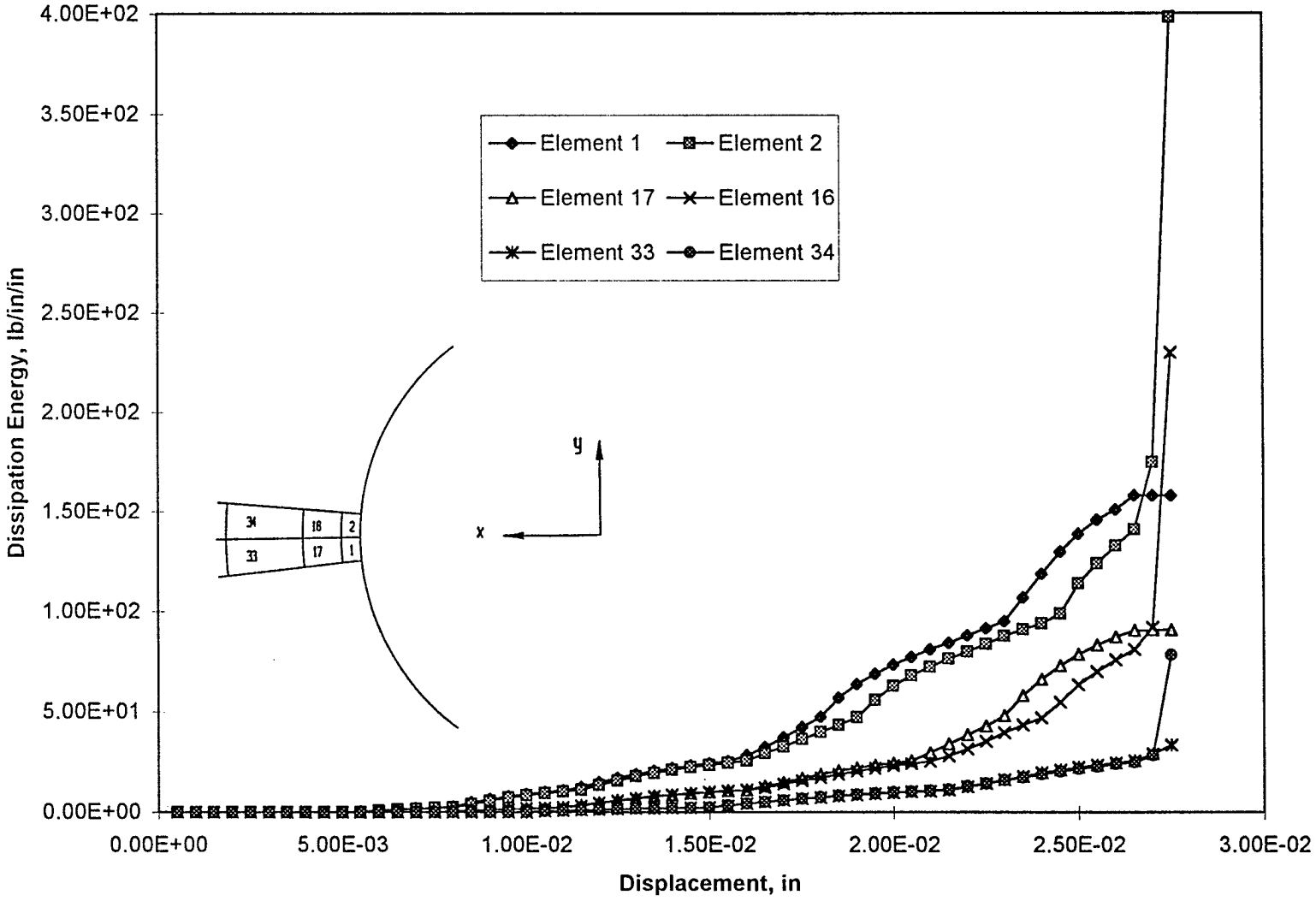

Figure 27. Dissipation Energy vs. Displacement for [0/45/-45/90]s with a 1/8" Hole, 90-Layer.

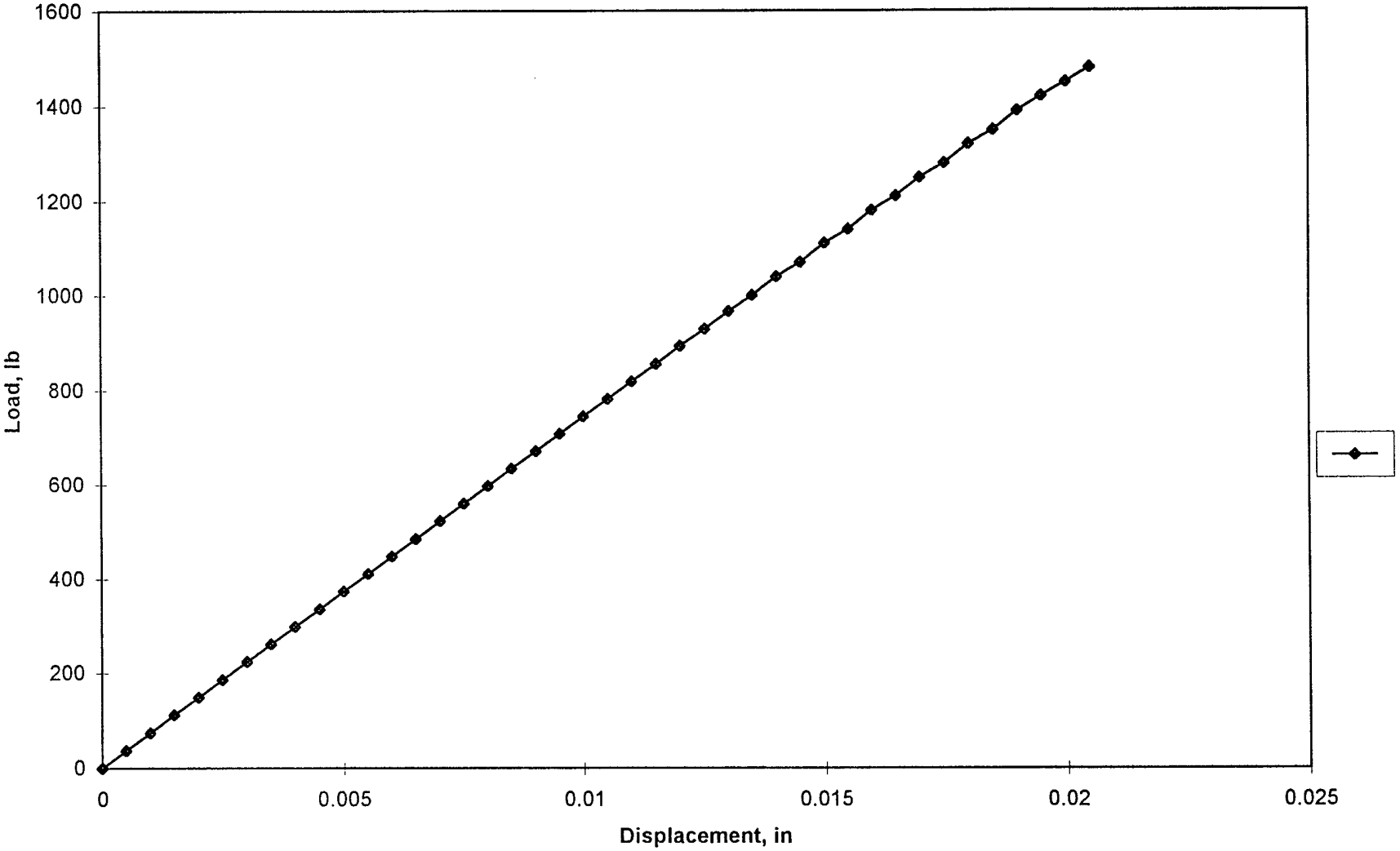

Figure 28. Load-Displacement Relation for [0/60/-60]s with a 1/4" Hole.

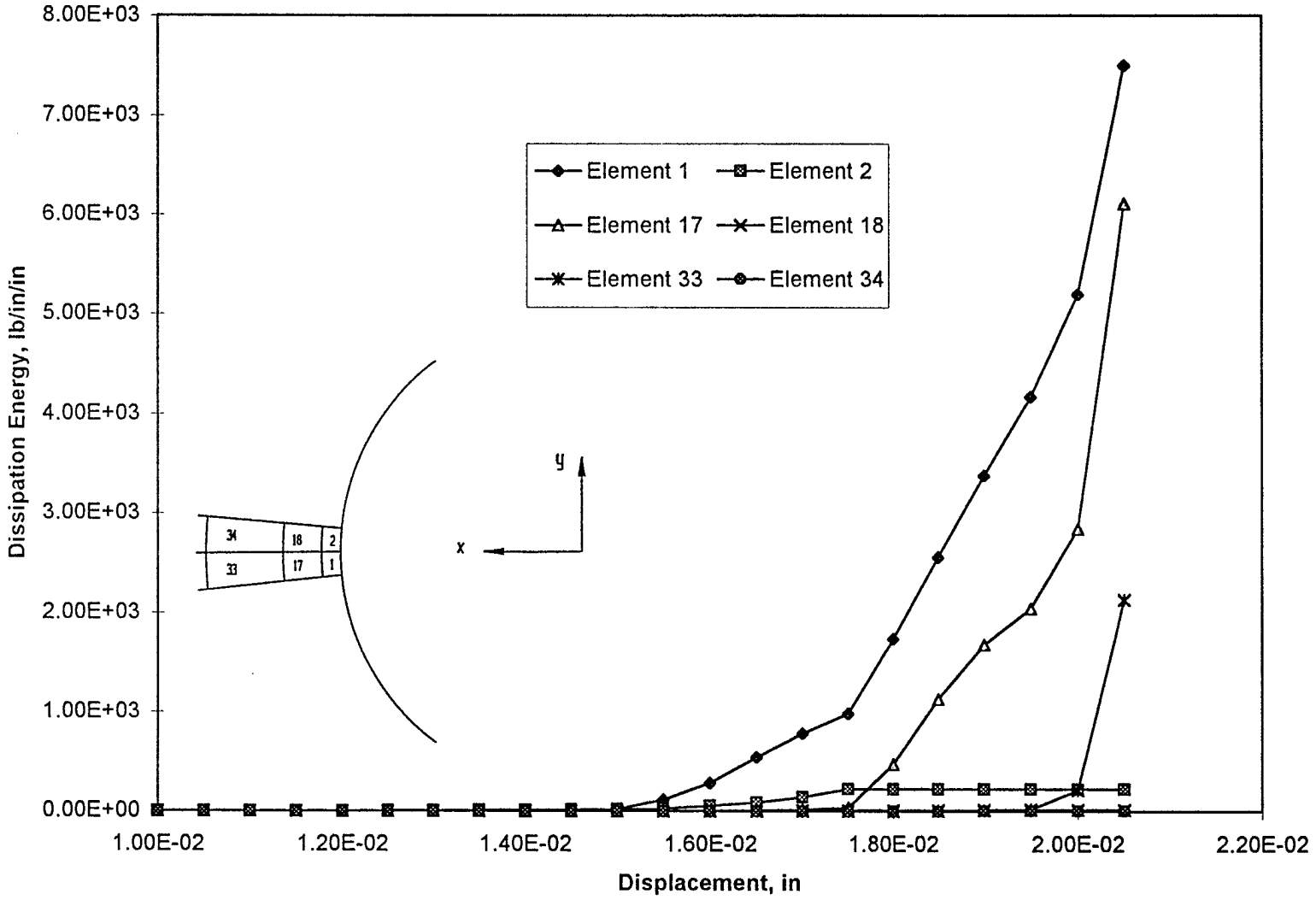

Figure 29. Dissipation Energy vs. Displacement for [0/60/-60]s with a 1/4" Hole, 0-Layer.

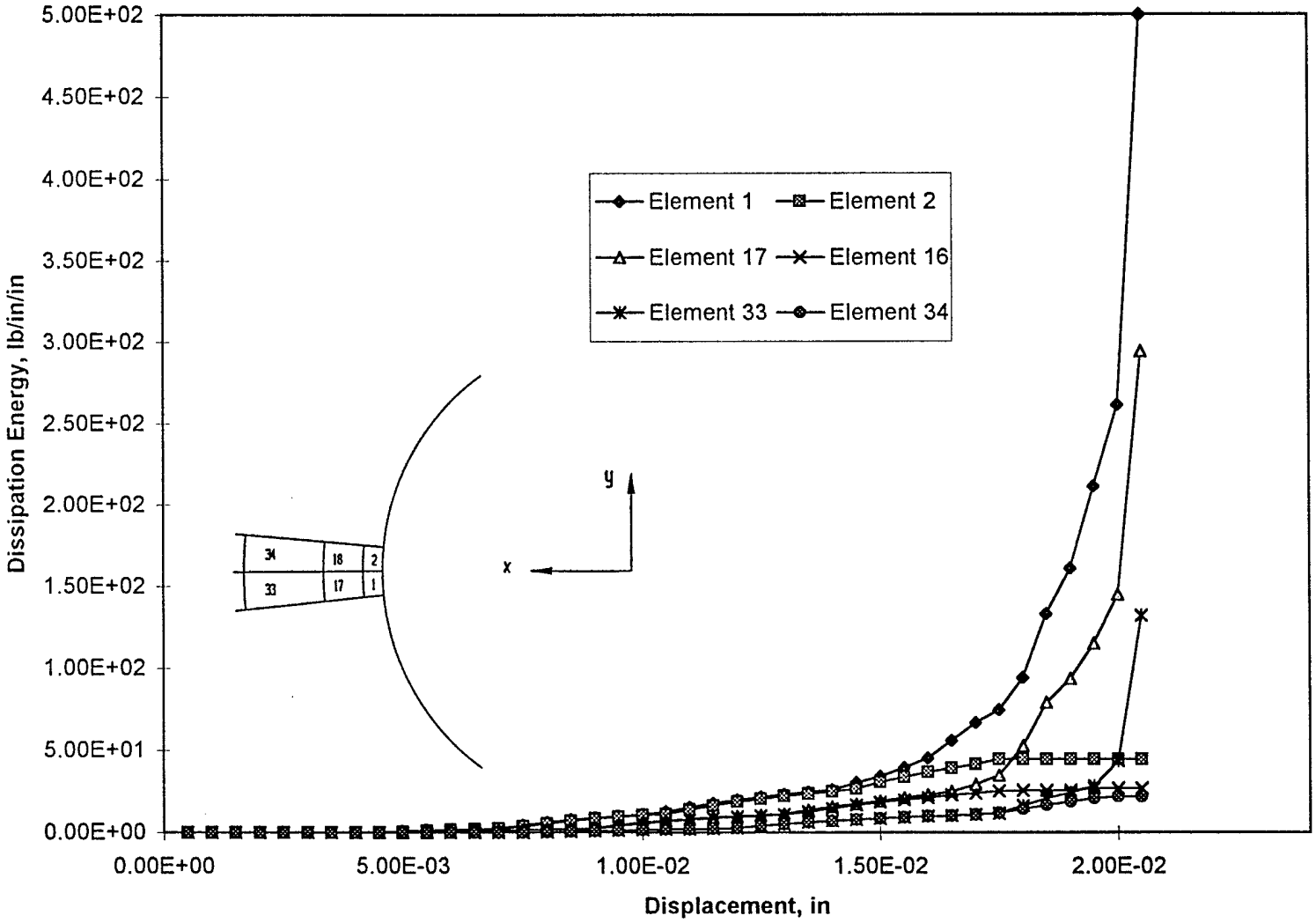

Figure 30. Dissipaation Energy vs. Displacement for [0/60/-60]s with a 1/4" Hole, 60-Layer.

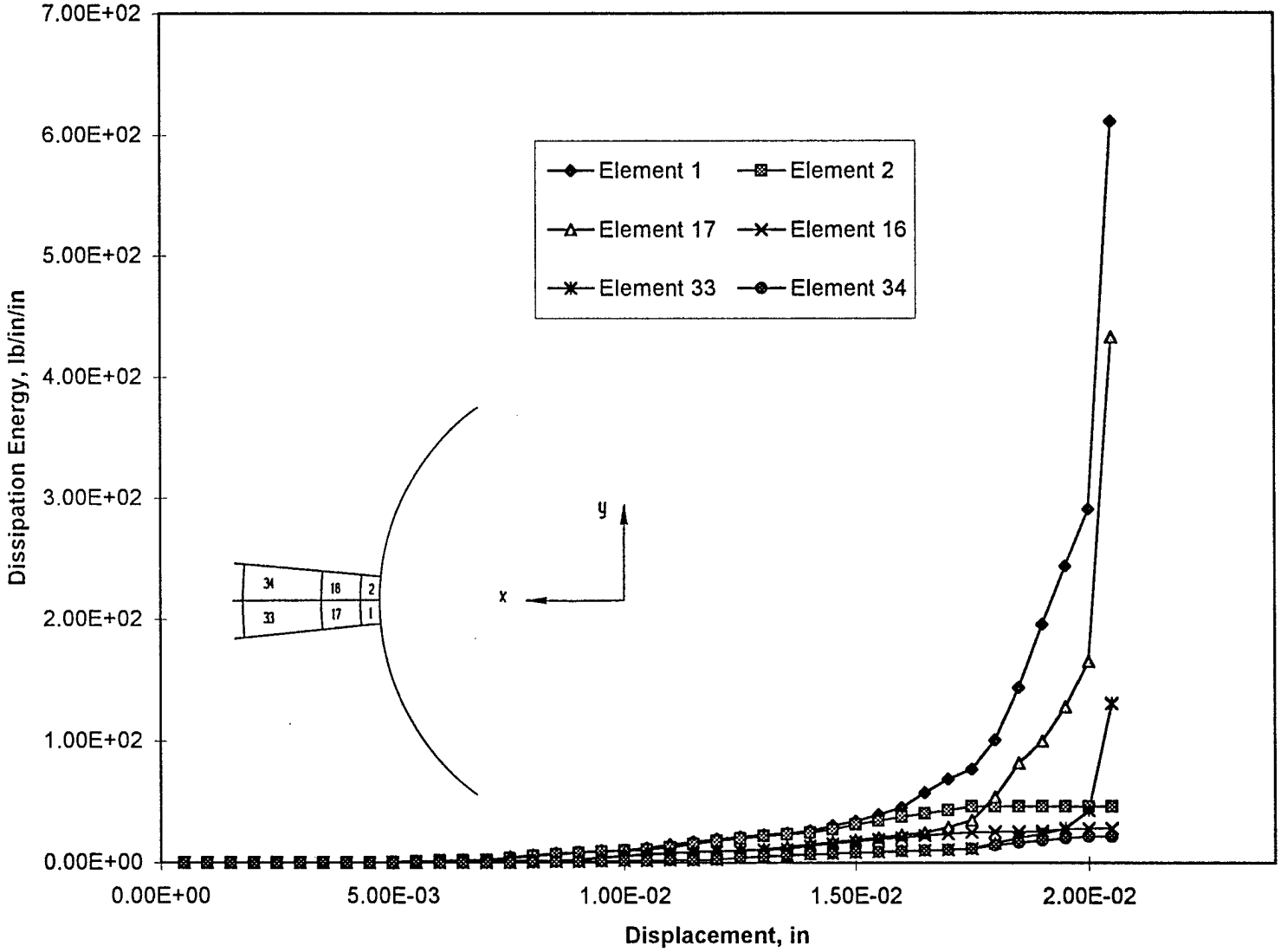

Figure 31. Dissipation Energy vs. Displacement for [0/60/-60]s with a 1/4" Hole, -60-Layer.

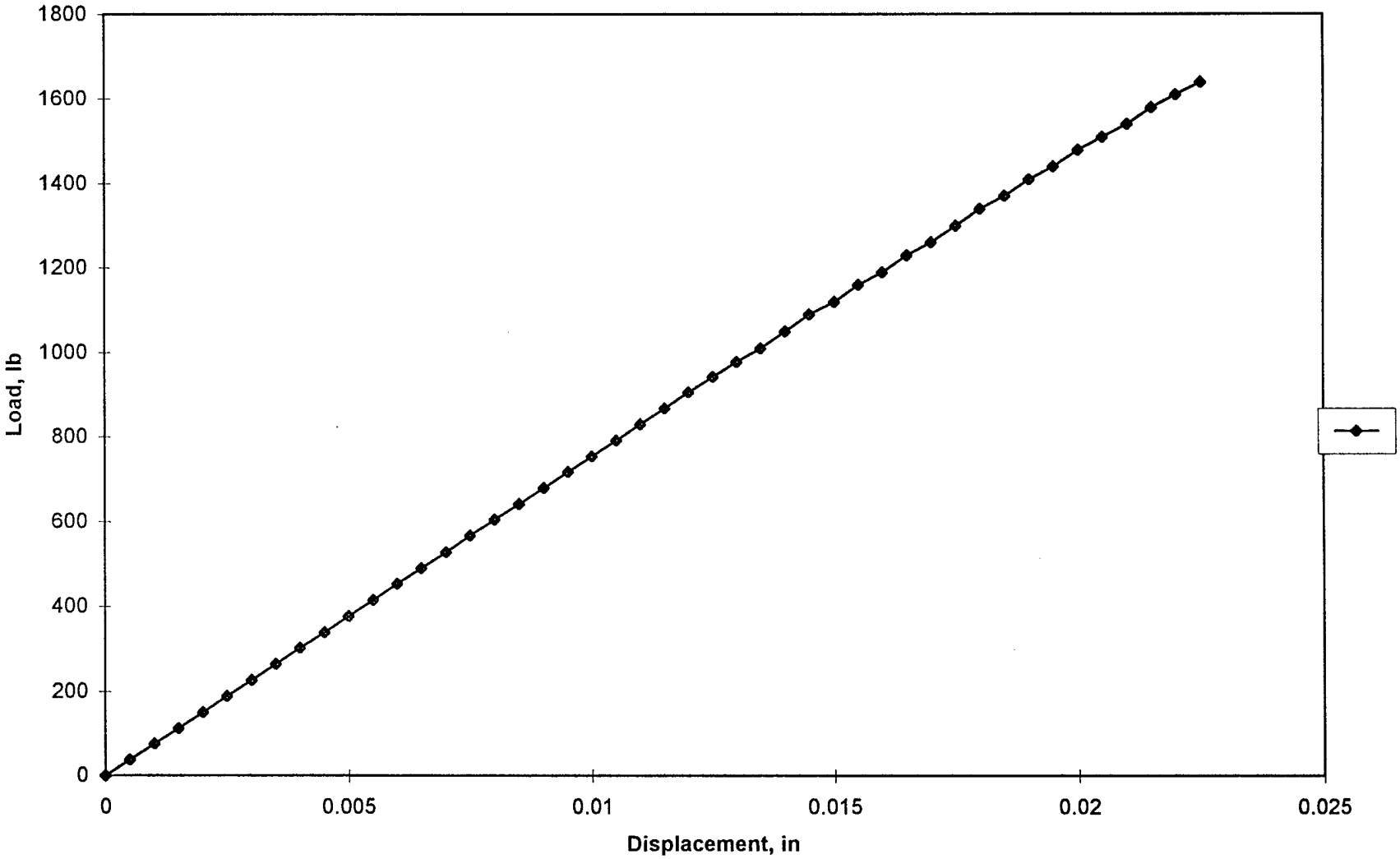

Figure 32. Load-Displacement Relation for [0/60/-60]s with a 1/8" Hole.

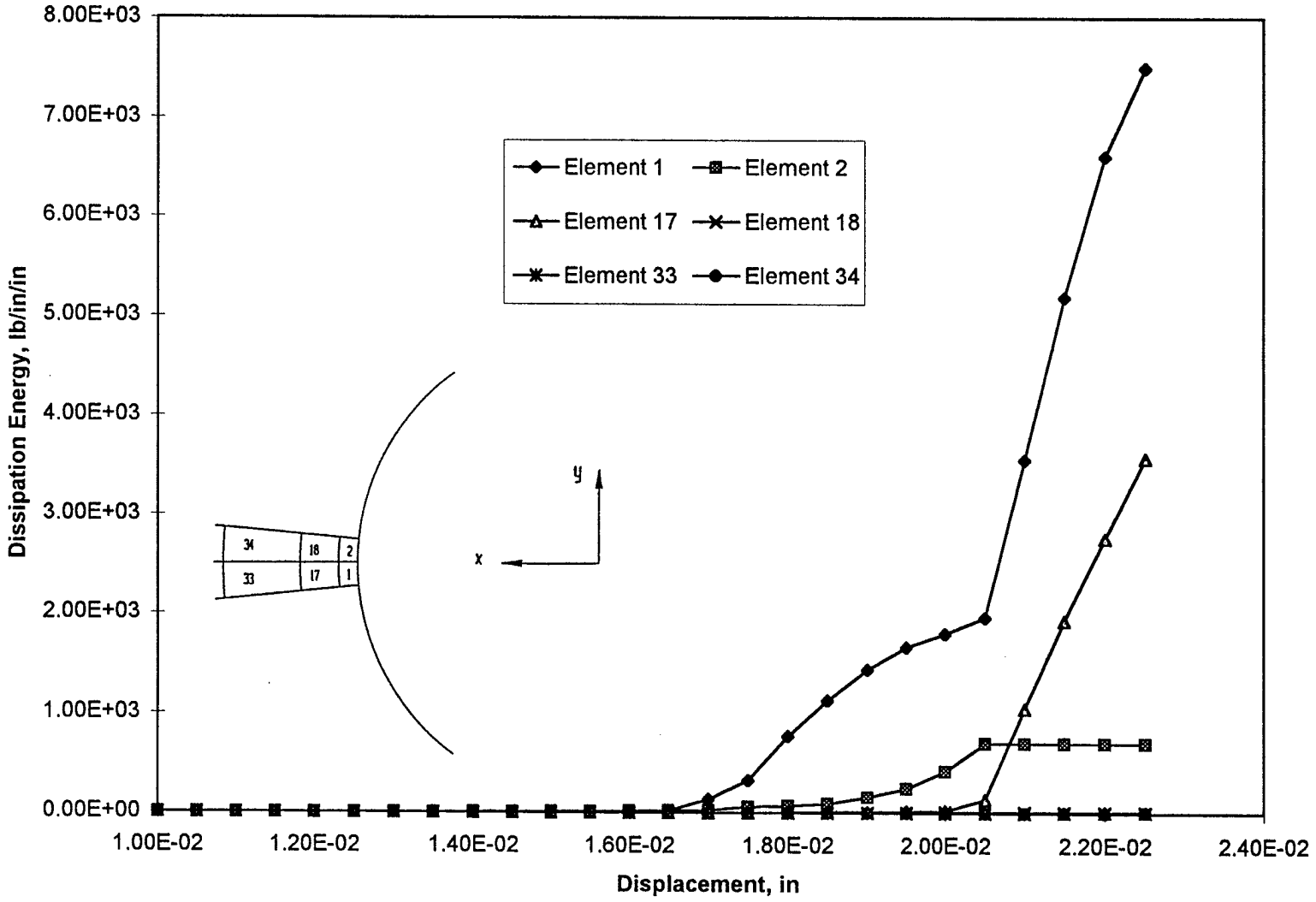

Figure 33. Dissipation Energy vs. Displacement for [0/60/-60]s with a 1/8" Hole, 0-Layer.

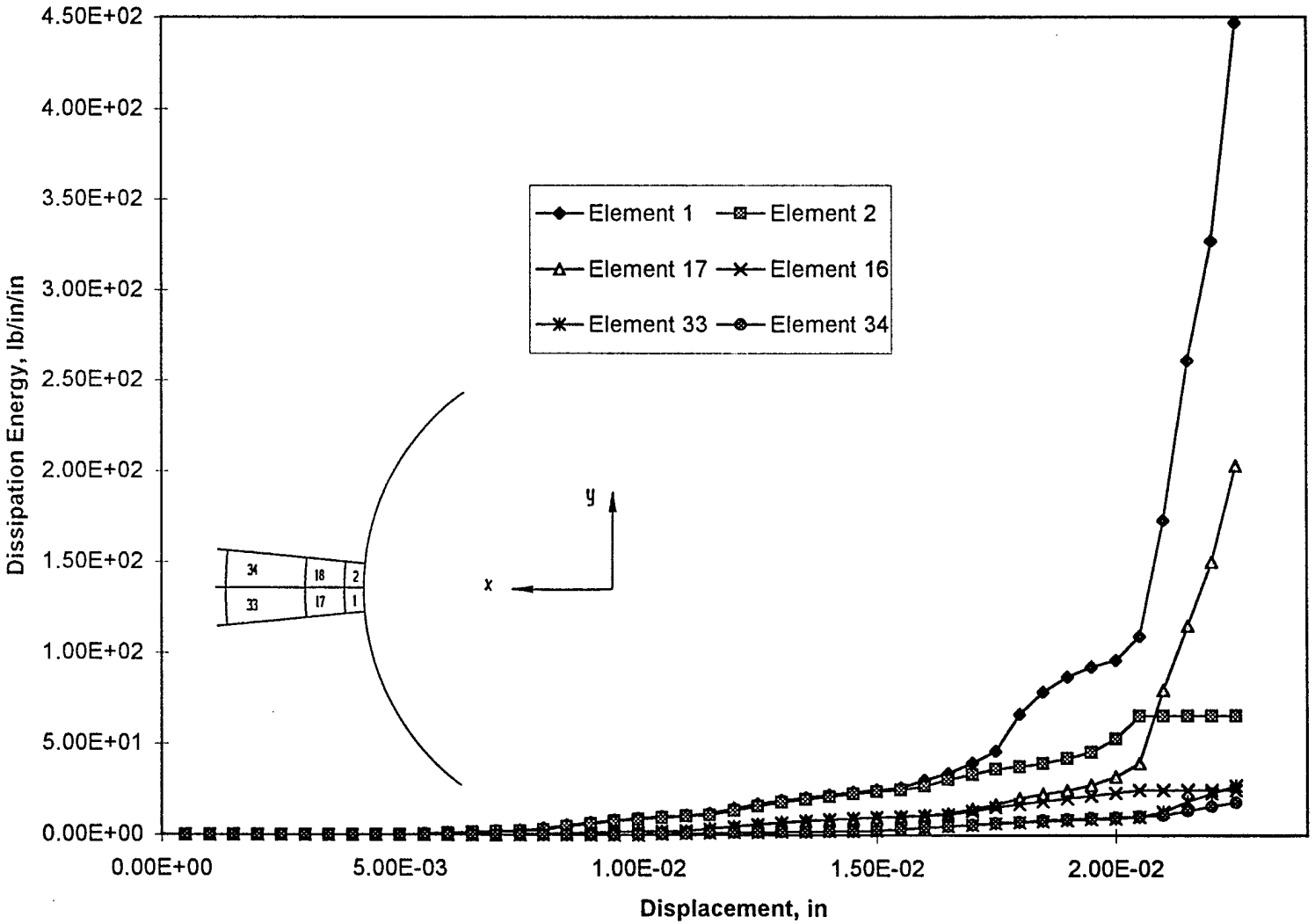

Figure 34. Dissipaation Energy vs. Displacement for [0/60/-60]s with a 1/8" Hole, 60-Layer.

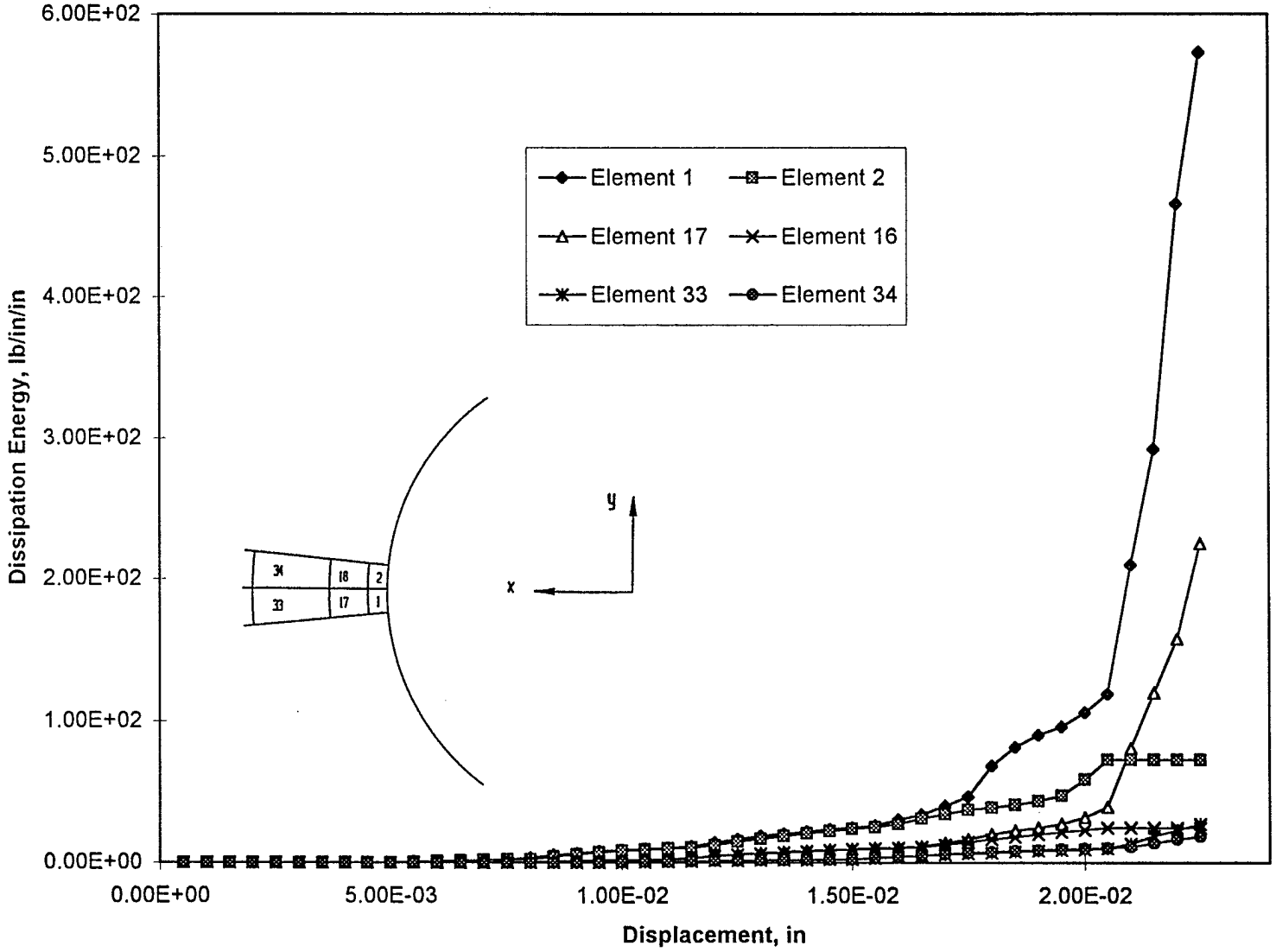

Figure 35. Dissipation Energy vs. Displacement for [0/60/-60]s with a 1/8" Hole, -60-Layer.

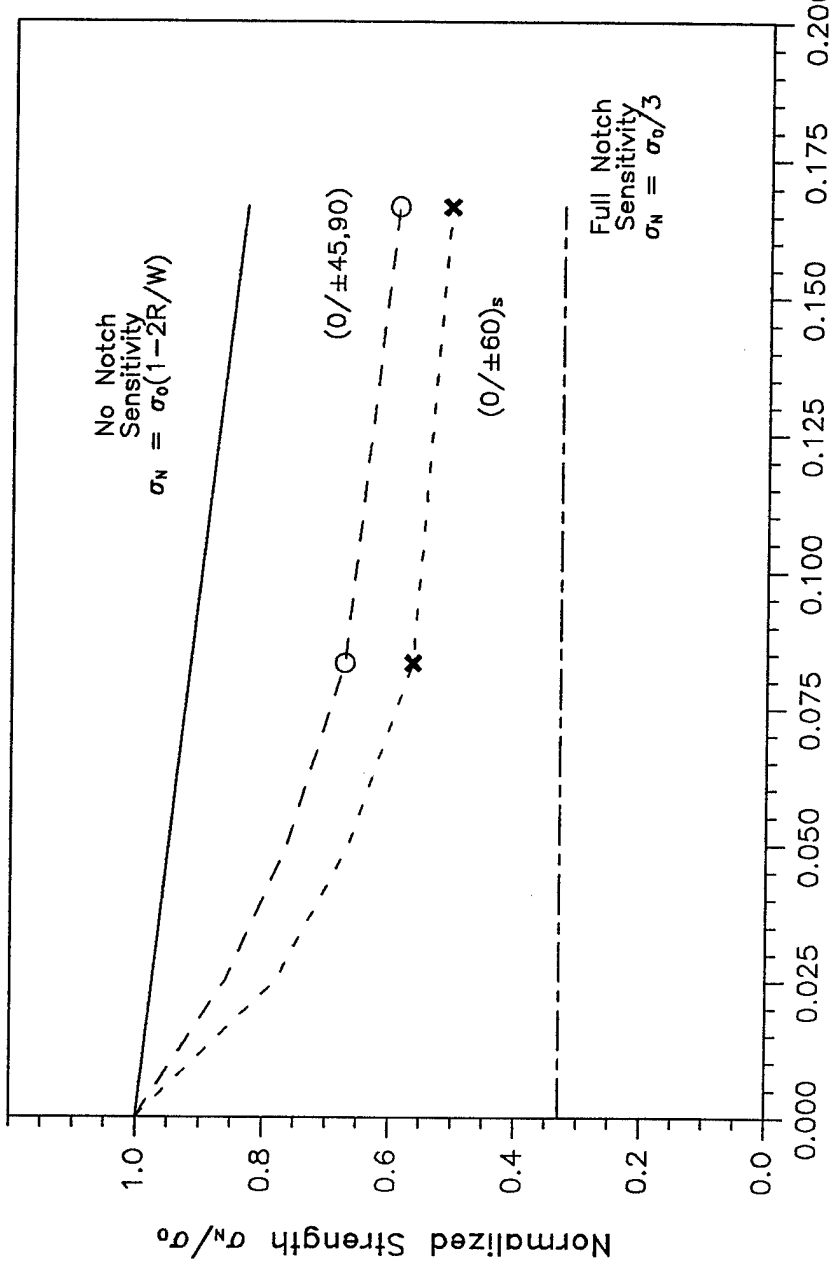

Figure 36. Calculated Normalized Gross Section Stress For Open Hole Tension.